
PANGENOME-BASED GENOME INFERENCE

Jana Ebler¹, Wayne E. Clarke², Tobias Rausch^{3,4}, Peter A. Audano⁵, Torsten Houwaart⁷, Jan Korbel³, Evan E. Eichler^{5,6}, Michael C. Zody², Alexander T. Dilthey⁷ and Tobias Marschall¹

¹*Institute for Medical Biometry and Bioinformatics, Heinrich Heine University Düsseldorf, Düsseldorf, Germany*

²*New York Genome Center, New York, New York, USA*

³*European Molecular Biology Laboratory (EMBL), Genome Biology Unit, Heidelberg, Germany*

⁴*European Molecular Biology Laboratory (EMBL), GeneCore, Heidelberg, Germany*

⁵*Department of Genome Sciences, University of Washington School of Medicine, Seattle, Washington, USA*

⁶*Howard Hughes Medical Institute, University of Washington, Seattle, Washington, USA*

⁷*Institute of Medical Microbiology and Hospital Hygiene, Heinrich Heine University Düsseldorf, Düsseldorf, Germany*

ABSTRACT

1 Typical analysis workflows map reads to a reference genome in order to detect genetic variants.
2 Generating such alignments introduces references biases, in particular against insertion alleles
3 absent in the reference and comes with substantial computational burden. In contrast, recent k-mer-
4 based genotyping methods are fast, but struggle in repetitive or duplicated regions of the genome.
5 We propose a novel algorithm, called PanGenie, that leverages a pangenome reference built from
6 haplotype-resolved genome assemblies in conjunction with k-mer count information from raw, short-
7 read sequencing data to genotype a wide spectrum of genetic variation. The given haplotypes enable
8 our method to take advantage of linkage information to aid genotyping in regions poorly covered
9 by unique k-mers and provides access to regions otherwise inaccessible by short reads. Compared
10 to classic mapping-based approaches, our approach is more than 4× faster at 30× coverage and at
11 the same time, reached significantly better genotype concordances for almost all variant types and
12 coverages tested. Improvements are especially pronounced for large insertions (> 50bp), where
13 we are able to genotype > 99.9% of all tested variants with over 90% accuracy at 30× short-
14 read coverage, where the best competing tools either typed less than 60% of variants or reached
15 accuracies below 70%. PanGenie now enables the inclusion of this commonly neglected variant type
16 in downstream analyses.

17 **Keywords** genotyping · pangenome · k-mers · haplotypes

18 **1 Introduction**

19 Diploid organisms have two copies of each autosomal chromosome, each of which can carry genetic variation. The
20 process of determining whether a known variant allele is located on one or both of these copies, or whether the variant
21 is absent in an individual's genome, is referred to as *genotyping*. Different classes of genetic variants exist and include
22 SNPs (single nucleotide polymorphisms), indels (insertions and deletions) up to 50 bp in size, and larger structural
23 variants (SVs). Large studies have produced comprehensive catalogues of known variation of various types, ranging
24 from single-nucleotide variants (SNVs) to large structural variants (SVs), for the human genome [1, 2, 3, 4]. Many
25 variants have been linked to diseases, such as schizophrenia or autism, which makes genotyping an essential task for
26 studying such diseases [5, 6, 7, 8, 9, 10]. Widely used genotyping methodss, such as GATK [11], FreeBayes [12], Delly
27 [13], Platypus [14] and SVTyper [15], are based on short-read alignments to a reference genome and thus, come with a
28 reference bias, as the aligner is unaware of possible alternative sequences that might be present in an individual's genome
29 [16, 17]. This can be especially problematic when genotyping structural variants, defined as events of 50bp and longer.
30 Recently, several approaches have been suggested that replace the linear reference genome by graph structures which
31 include possible alternative alleles. Graphs are either built from given variant calls or haplotype-resolved assemblies,
32 and genotypes are derived from alignments of sequencing reads to these graphs [18, 17, 19, 20, 21]. In general, these
33 graph-based approaches were shown to improve genotyping accuracy over methods that rely on a linear reference
34 genome by reducing reference bias. However, aligning sequencing reads is a time consuming task even for linear

35 reference genomes, where mapping $30\times$ short read sequencing data of a single sample takes around 100 CPU hours.
36 This problem is amplified when transitioning to graph-based pangenome references, where the read mapping problem
37 is even more computationally expensive.
38 A much faster alternative is to genotype known variants based on counts of k -mers, short sequences of a fixed length k ,
39 in the raw sequencing reads. Cortex [22] was the first approach to genotyping variants leveraging read k -mer count
40 information based on a colored de Bruijn graph constructed from sequencing data and known allelic sequences. Dilthey
41 et al. [23] use a similar idea and construct population reference graphs from known haplotype sequences to genotype a
42 sample's MHC region based on short read sequencing data, but this approach does not scale to whole genomes.
43 Dolle et al. [24] genotype SNPs and short indels based on querying reads containing allele specific k -mers in the
44 data. They derive genotypes from alignments of these reads to reference and alternative sequences. BayesTyper [25]
45 constructs graphs containing reference and alternative alleles for sets of variants that are less than a k -mer size apart in
46 the genome and genotypes are computed by sampling the likeliest pair of local haplotypes through each such cluster of
47 variants, based on the observed k -mer count profiles. Such k -mer-based methods allow fast genotyping by bypassing
48 the time consuming alignment step. However, they can struggle in repetitive and duplicated regions of the genome
49 which are not covered by any unique k -mers, as they lack the connectivity information contained in the reads. This is
50 especially problematic for structural variants which are often located in repeat-rich or duplicated regions of the genome
51 [26, 3].
52 Turner et al. [27] aim to address this problem by introducing linked de Bruijn graphs which store long range connectivity
53 information from sequencing reads on top of a de Bruijn graph. They demonstrated that adding link information from a
54 set of reference sequences to the graph in this way improved drug resistance locus assembly in *K.pneumoniae* isolates.
55 In a similar manner, information of already known haplotype sequences of other samples could improve k -mer-based
56 genotyping especially in difficult to access regions of large diploid genomes, but methods for this have so far been
57 lacking. Known haplotypes (in form of a reference panel) have been used previously for population based phasing of a
58 small variants. The Li-Stephens Model provides a theoretical framework by formulating this problem in terms of a
59 Hidden Markov Model [28]. Furthermore, reference panel information can be used to impute missing genotypes of a
60 sample [29, 30, 31, 32], but accurate SV-integrated reference panels have been challenging to construct.
61 Recently, single molecule sequencing technologies delivering long read data have enabled breakthroughs in producing
62 *de novo* haplotype-resolved genome assemblies [33, 34, 35]. Such assemblies are already available for several human
63 samples and major efforts are underway¹ to generate hundreds of human genome assemblies with the intention of
64 deriving a pangenome representation that replaces the current reference genome GRCh38. So far, however, scalable
65 methods to leverage such haplotype-resolved pangenome representations for the interpretation of short-read data sets
66 are not available.
67 In this paper, we describe an algorithm, PanGenie (for *Pangenome-based Genome Inference*), that makes use of
68 haplotype information from an assembly-derived pangenome representation in combination with read k -mer counts for
69 efficiently genotyping a wide spectrum of variants. That is, our method is able to leverage the information inherent in
70 the assemblies in order to infer the genome of a new sample for which only short-reads are available. PanGenie bypasses
71 read-mapping and is entirely based on k -mers, which allows it to rapidly proceed from the input short reads to a final
72 call set including SNPs, indels and structural variants, enabling access to variants typically not accessible in short-read
73 workflows – such as larger insertions. We applied our method to genotype variants called from haplotype-resolved
74 assemblies of six individuals, revealing a substantial advance in terms of runtime, genotyping accuracy, and in the
75 number of accessible variants.

76 2 Results

77 2.1 Algorithm overview

78 The input to our algorithm consists of short read sequencing data for the sample to be genotyped, a reference genome,
79 as well as a pangenome graph containing variants and paths representing known haplotype sequences. The latter is
80 represented in terms of a fully-phased, multisample VCF file. In a first step, clusters of variants less than the k -mer
81 size apart are combined into single, multi-allelic variants. We identify all k -mers unique to a variant region, that is,
82 k -mers that cover the variant position and do not occur anywhere else in the genome, and use Jellyfish [36] to determine
83 their counts in the reads. Our genotyping model combines two sources of information in order to derive genotypes for
84 the variants: read k -mer counts and the already known haplotype sequences. The distribution of k -mer counts along
85 the allele paths of a variant can hint towards the genotype of the sample. Figure 1a provides an example: three alleles

¹<https://www.genome.gov/news/news-release/NIH-funds-centers-for-advancing-sequence-of-human-genome-reference>

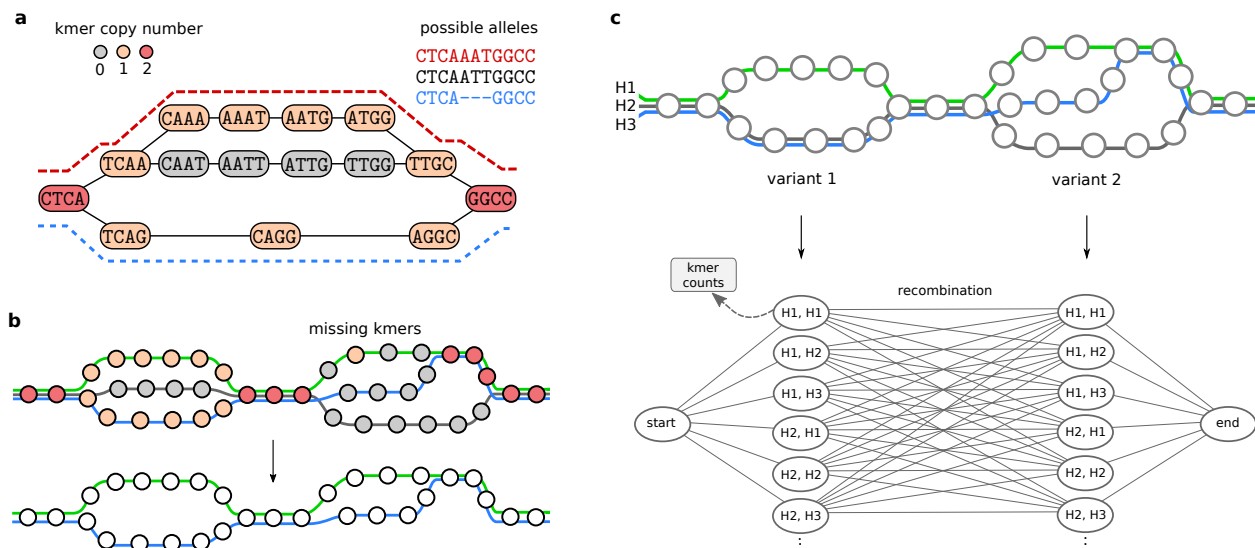


Figure 1: **Genotyping approach.** Our genotyping algorithm combines two sources of information: read k-mer counts and known haplotypes. **a)** A variant region in the constructed genome graph is shown. Each path corresponds to an allele. Colors indicate copy number estimates for the k-mers, based on which a genotype can be determined. Here, the variant likely carries the red and the blue allele, indicated by the two dashed lines. **b)** A larger proportion of the graph is shown, with three known haplotypes threaded through it. Again, colors indicate copy number estimates. The second bubble is poorly covered by k-mers, however, linkage to adjacent variants can be used to infer the two local haplotype paths. **c)** A genome graph with two variant positions is shown with the corresponding HMM below. Gray circles in the graph indicate k-mers. The hidden states of the HMM correspond to possible pairs of the three haplotype paths shown in the graph. These states output counts for unique k-mers characterizing the alleles.

86 are shown for a variant. All k-mers corresponding to the middle one are absent from the reads of the sample. This
 87 indicates that the individual carries the red and the blue allele at this position. However, variants may be poorly covered
 88 by k-mers, or no unique k-mers may exist for a variant in repetitive regions of the genome. Such positions cannot be
 89 reliably genotyped by an approach based purely on the k-mer counts. In these regions, information of known haplotype
 90 sequences of a population can help to infer genotypes based on neighboring variants. An example is provided in Figure
 91 1b: known haplotype sequences can be represented as paths in the graph. The second variant is poorly covered by
 92 k-mers but the count distribution of k-mers along the alleles of the first variant indicates that the unknown genome is
 93 composed of the green and blue haplotype.

94 For genotyping, we combine these two sources of information by constructing a Hidden Markov Model which models
 95 the unknown haplotypes of a sample as mosaics of the provided haplotypes and reconstructs them based on the read
 96 k-mer counts observed in the sample's sequencing reads. To achieve this, our HMM has a hidden state for each possible
 97 pair of given haplotypes that can be chosen at each variant position. These states emit counts for the unique k-mers in
 98 the variant region based on the copy number of these k-mers in the two selected haplotypes. Changes in the selected
 99 haplotype paths between adjacent variant positions correspond to recombination events. Therefore, we define transition
 100 probabilities based on recombination probabilities defined in [28]. We show an example in Figure 1c. Running the
 101 Forward-Backward algorithm, we can compute genotype likelihoods for each position, from which we finally derive a
 102 genotype. Using the Viterbi algorithm, we can compute the two likeliest haplotype sequences given the observed k-mer
 103 counts.

104 2.2 Constructing a pangenome reference from haplotype-resolved assemblies

105 In order to construct a pangenome graph, we used haplotype-resolved assemblies of five individuals that have recently
 106 been produced [34, 35]. These samples include two individuals of Puerto Rican descent (HG00731, HG00732) as well
 107 as NA12878, NA24385 and PGP1. For each sample, we separately mapped contigs of each haplotype to the reference
 108 genome and used these alignments to call variants on each haplotype of all autosomes (see 4.1 for details). In order to
 109 filter out low quality or erroneous calls, we only kept variants located in regions in which all haplotypes were covered
 110 by exactly one contig alignment. These *callable* regions cover 87.42% (2.51 Gb) of chromosomes 1-22.

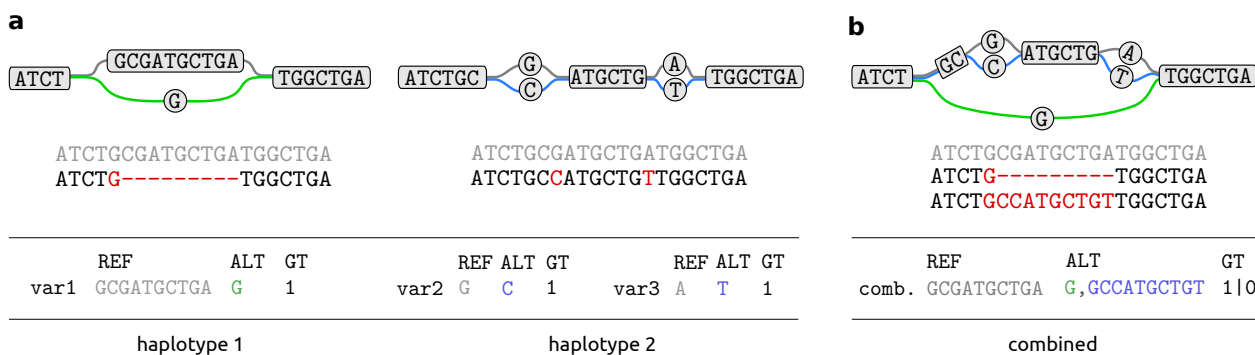


Figure 2: **Combining variant calls.** a) Shown are alignments of two contigs to the reference genome and variant calls for both of them: a deletion for the contig of the first haplotype, and two SNPs for the second haplotype. Additionally, the pangenome graphs that result from inserting these variants into the reference genome, are shown. b) Variant calls of both haplotypes are overlapping and will be represented as a single bubble when constructing a graph that contains all variants. In the resulting VCF, only those paths through the bubble will be listed, that were observed in at least one of the input haplotypes and additionally, the genotypes corresponding to each sample.

111 We create an acyclic and directed pangenome graph that contains bubbles representing the variation observed in all of
 112 the input haplotypes. Variants overlapping across haplotypes are combined into a single bubble with potentially multiple
 113 branches reflecting all allele sequences observed in the respective genomic region. The input haplotypes are represented
 114 as paths through the resulting pangenome. The final graph is represented in terms of a fully phased, multi-sample VCF
 115 file. Figure 2 provides an example of how we construct the graph.

116 Due to the lack of haplotyped-resolved assemblies for other samples, the number of haplotype paths in our graph is
 117 relatively small. Until more assemblies become available in the future, we showcase the performance of our method
 118 by extending our pangenome reference panel using additional short read data sets. To this end, we apply PanGenie to
 119 phase the same set of variants in these additional samples. In this way, we used short-read sequencing data of a sample
 120 of Chinese descent, one individual of Yorubian descent as well as four samples from different populations (see Figure
 121 3a and Section 4.1) in order to produce an “extended” panel consisting of eleven samples.

122 We present callset statistics in Figure 3. The transition/transversion (ti/tv) ratio for SNPs and the heterozygous/homozygous ratio are commonly used quality control measures for callsets [37, 38]. The ti/tv ratio is expected to
 123 be around two as transitions (changes from A to G, G to A, C to T and T to C) are twice as frequent as the remaining
 124 transversions. The distribution of these substitution types for our SNP calls are shown in Figure 3b. We computed
 125 ti/tv ratios between 2.04 and 2.05 for all of our samples. Theoretically, the expected het/hom ratio for a callset is two
 126 for variants in Hardy-Weinberg equilibrium [37]. However, it has been previously reported to vary by ancestry and was
 127 observed to be smaller for individuals of American, Asian and European origin [38, 39]. This is in line with what we
 128 observe for our callsets. The five samples from which variant calls were generated are of American or European origin.
 129 We observed het/hom ratios between 1.56 and 1.67 for all these individuals (Figure 3a). Additionally, we show detailed
 130 counts observed for SNPs, insertions, deletions and complex variants of different lengths in Supplementary Table 2.
 131 Insertions and deletions include only bi-allelic variants, other types of structural variants or multi-allelic variants (that
 132 are not SNPs), are defined as complex variants. We distinguish small variants (1 – 19bp), midsize variants (20 – 50bp)
 133 and large variants (> 50bp). The total number of calls in each category can be found in Supplementary Table 3d. We
 134 additionally re-run our variant calling using reference version hg19 in order to be able to compare the resulting variant
 135 calls to the structural variants (> 50bp) contained in the Genome Aggregation Database (gnomAD) [4]. We found an
 136 overlap of 6,398 variants. 21,370 positions were only contained in our assembly-based callset set (see Supplementary
 137 Section 4.3).
 138

139 2.3 Genotyping evaluation

140 For evaluation, we conducted a “leave-out-one experiment” and genotyped each of the four unrelated samples HG00731,
 141 HG00732, NA12878 and NA24385 based on Illumina reads from the HGSVC [3], the Genome in a Bottle Consortium
 142 [40] and 1000 Genomes Project high-coverage data (Mike Zody, personal communication). We used the variants from
 143 the pangenome graph constructed in Section 2.2 and two different sets of haplotype paths from this graph as input to
 144 our genotyping algorithm: first we only used the haplotypes that we obtained from haplotype-resolved assemblies,
 145 second, we added haplotypes from our extended callset. Thus, the former small panel consists of haplotypes for
 146 samples: HG00731, HG00732, NA12878, NA24385 and PGP1. The latter, extended panel, additionally contains

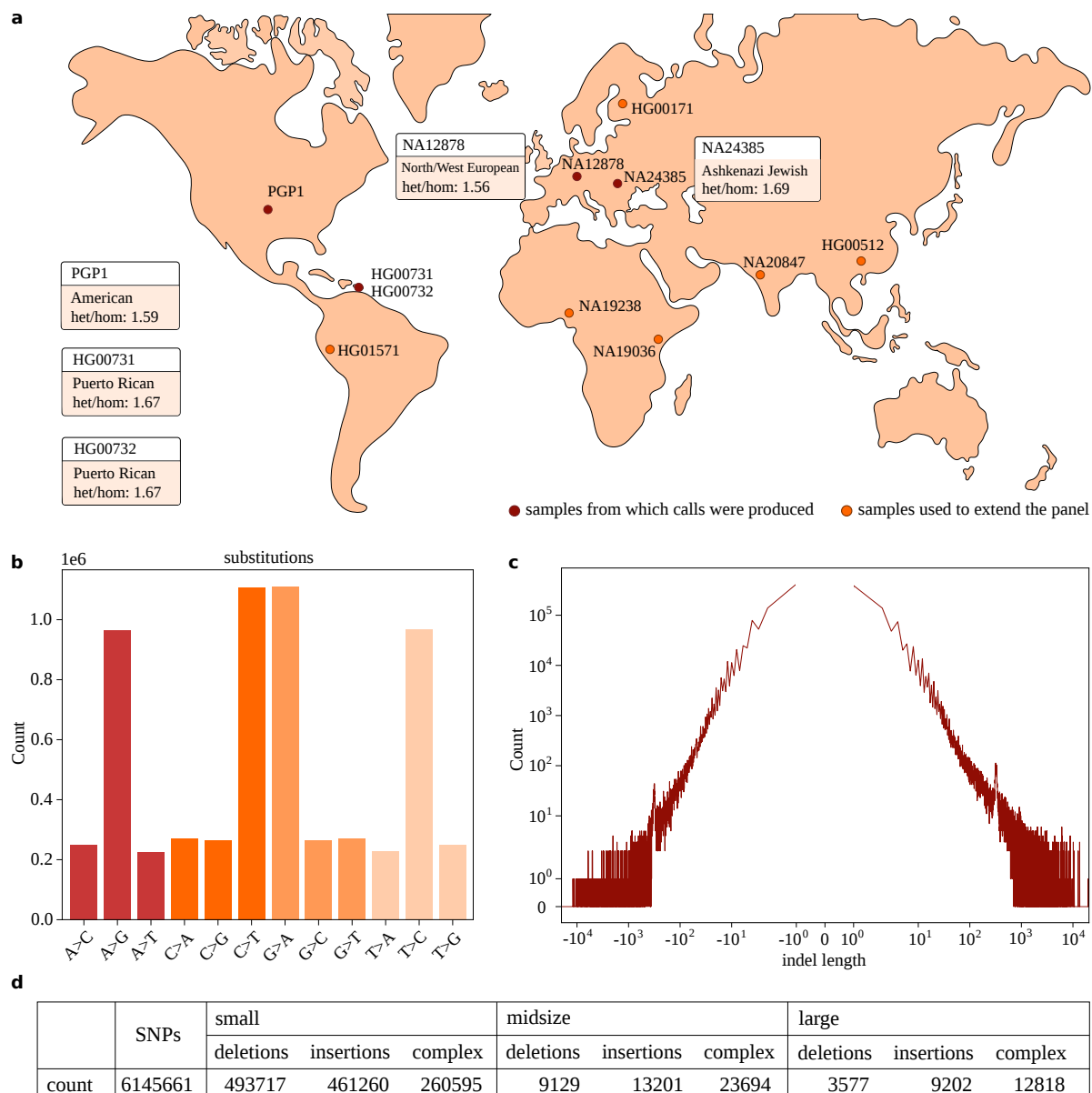


Figure 3: **Callset statistics.** Statistics for variants called from haplotype-resolved assemblies. **a)** Samples for which variants were called from haplotype-resolved assemblies are shown in red, as well as the population they originate from and the het/hom ratio observed for the variant calls. Furthermore, samples used to extend the panel are shown (orange). **b)** Shown are the number of different substitutions reported for all samples. **c)** Length distribution of insertions and deletions across all samples. Deletion lengths are reported as negative numbers, insertion lengths are positive. **d)** Number of variants per category: small (1 – 19bp), midsize (20 – 50bp), and large (> 50bp). Insertions and deletions include only bi-allelic variants, other types of structural variants or multi-allelic variants (that are no SNPs).

147 haplotypes of: HG00512, NA19238, NA20847, NA19036, HG00171 and HG01571. We genotyped each of the four
 148 samples in a leave-one-out manner by removing it from the small and extended panels, respectively, and genotyped it
 149 based on the remaining samples. We then compare the genotype predictions to the ones of the left out, ground truth
 150 haplotypes derived from the haplotype-resolved assemblies. We additionally ran Platypus [14], BayesTyper [25], GATK
 151 HaplotypeCaller [11] and Paragraph [20] for comparison. Since Platypus, GATK and Paragraph are mapping-based
 152 approaches and require BAM-files as input, we used bwa mem [41] to align the reads to the reference genome prior to
 153 genotyping. PanGenie and BayesTyper are k-mer-based and were provided with the raw, unaligned sequencing reads
 154 (in FASTQ-format). We ran our experiments on different levels of read coverage. For this purpose we downsampled the

155 reads of each sample to coverages $30\times$, $20\times$, $10\times$ and $5\times$. Not all tools can handle all types of variants. We ran GATK
156 only on SNPs, small and midsize variants and Paragraph was only run on midsize and large variants.

157 **Evaluation metrics.** Given a truth set of variants with known genotypes and genotype predictions made by a
158 genotyper for these positions, we compute two metrics in order to evaluate the genotyping performance. The first one is
159 the percentage of variants for which a tool was able to give a genotype prediction. Ideally, this fraction should be as
160 large as possible. The second one is the *genotype concordance* that we define as the percentage of correct genotype
161 predictions among all variants that were typed by the method.

$$\text{genotype concordance} = \frac{\text{correct predictions}}{\text{correct predictions} + \text{wrong predictions}} \cdot 100 \quad (1)$$

162 **Results.** We show the genotyping results for sample HG00731 that we obtained from PanGenie using the extended
163 panel as well as from the remaining methods in Figure 4 and 5. Respective results for the three other samples are
164 similar and can be found in Supplementary Figures 8-13. The results we got from using the small panel are presented in
165 Supplementary Figures 14-21. The plots show the genotype performances outside and inside of STR/VNTR regions,
166 which we obtained from the UCSC genome browser [42]. We observed that between 54 – 78% of midsize and large
167 variants are indeed located inside of repeats (Supplementary Table 3). Like most genotyping tools, PanGenie also
168 calculates a phred-scaled genotype quality score which can be used to filter the genotypes. In our evaluation, we
169 consider two configurations for PanGenie: “lenient” filtering, where we do not apply any filter and use all reported
170 genotypes, and “strict”, where we only used high quality genotype predictions (quality ≥ 200) and treat all other
171 variants as not genotyped. For all other tools, we did not apply any filters on the genotype quality and used all genotypes
172 that they reported.

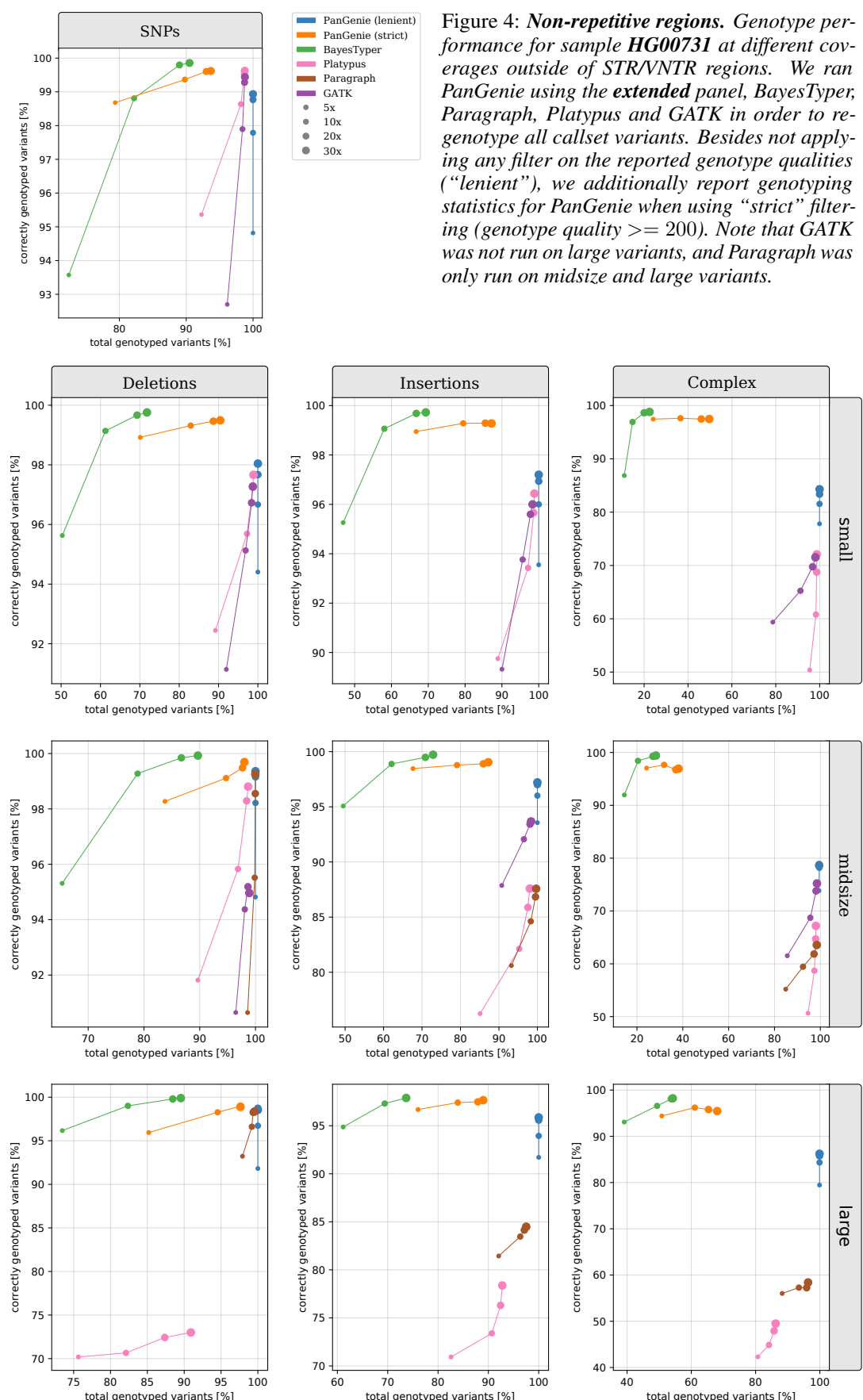
173 For SNPs, all methods reach similar levels of genotype concordances. Platypus and PanGenie (small + extended panel)
174 perform best on the lowest tested coverage of $5\times$. While PanGenie is able to genotype almost all variants ($> 99.998\%$)
175 using “lenient” filtering on high and low coverage, the other methods show larger levels of variants that they leave
176 untyped. This is especially the case for BayesTyper, which reaches higher levels of genotype concordances than the
177 other tools at coverages $10 - 30\times$, but does not genotype 9% of the SNPs outside of STR/VNTR regions, and 40%
178 inside these repeat regions at coverage $30\times$ for sample HG00731.

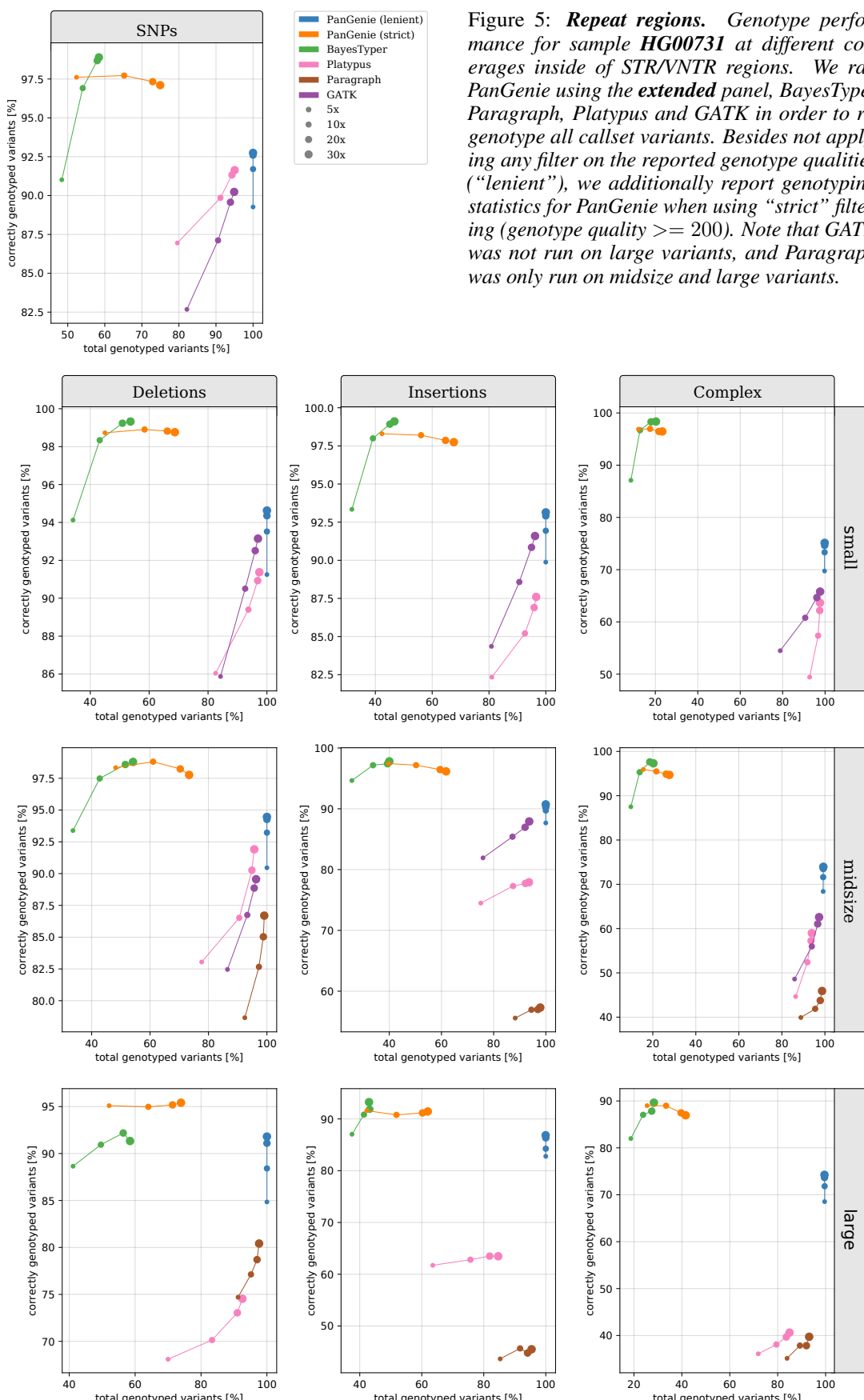
179 For the small variants, PanGenie outperforms the mapping-based approaches on most coverages using the small panel.
180 With the extended panel, we can improve the performance of our method even further, especially inside of STR/VNTR
181 regions. Here, PanGenie reaches genotype concordances superior by 6.5%, 6.26% and 28% compared to the best
182 performing mapping-based approach on insertions, deletions and complex variants, respectively, when using the “lenient”
183 model. BayesTyper produces higher percentages of correct predictions, but is not able to determine genotypes for
184 30 – 90% of the variants outside of repeat regions, and between 50 – 91% of variants located inside of STR/VNTR
185 regions. Using “strict” filtering, PanGenie is able to reach genotype concordances similar to BayesTyper, while still
186 being able to type much larger fractions of variants.

187 We observe a similar trend for midsize and large variants as well. Here, PanGenie clearly outperforms the mapping-
188 based tools even when using the small panel of haplotypes. Improvements were largest for large variants inside of repeat
189 regions, where PanGenie with the extended panel and “lenient” filtering is able to reach genotype concordances that are
190 up to 15%, 37% and 89% higher than those of the best performing mapping-based approach for insertions, deletions
191 and complex variants, respectively. The percentages of large variants that could not be genotyped by BayesTyper is
192 between 60 – 80% in all cases, while PanGenie types more than 99% of the variants in each category in “lenient” mode.

193 When restricting the evaluation to variants contained in the Genome in a Bottle (GIAB) small variant calls [43],
194 PanGenie showed genotyping performances similar to the other methods, while outperforming them on the lowest
195 tested coverage of $5\times$ (Supplementary Section 4.3).

196 In general, genotyping longer variants based on short-read data is a challenging task, since such variants are often
197 located in repetitive or duplicated regions of the genome [26]. Their short length makes it difficult to unambiguously
198 map the reads in these regions which also effects the genotyping process that relies on these alignments. K-mer based
199 approaches additionally lack the connectivity information contained in the reads, which makes genotyping variants in
200 such difficult regions even more complicated. This is one possible explanation why we observed such high numbers of
201 untyped variants for BayesTyper. PanGenie overcomes these limitations of short reads, as it additionally incorporates
202 long-range haplotype information inherent to the pangenome reference panel it uses. This enables imputation of
203 genotypes in regions poorly covered by k-mers and helps to improve genotyping performance over the other methods,
204 especially for midsize and large variants located in repetitive regions of the genome.





205 **Runtimes.** Runtimes (in CPU hhh:mm:ss) of all methods for sample HG00731 are shown in Table 1. The runtimes
206 for the other samples were very similar and are provided in Supplementary Table 4. For each method, we measured
207 the time required to produce genotypes given an input set of variants and raw, unaligned sequencing reads. Since
208 k-mer based methods PanGenie and BayesTyper bypass the time-consuming read alignment step, they are much faster
209 compared to the remaining, mapping-based methods. GATK and Paragraph were the slowest methods, although they
210 were – unlike the other tools – only run on a subset of variants. PanGenie in contrast, was the fastest method on all
211 coverages. Using the small panel, it was between $3.3 - 3.56 \times$ faster than Platypus on the lowest tested coverage of $5 \times$,
212 and between $6.52 - 8.21 \times$ faster on coverage $30 \times$. Using the extended panel, these numbers were $1.07 - 1.25 \times$ and
213 $4.03 - 4.27 \times$, respectively.

method	coverage			
	$5 \times$	$10 \times$	$20 \times$	$30 \times$
PanGenie-4	5:43:14	7:13:16	10:34:05	14:41:47
PanGenie-10	16:30:46	18:38:24	21:58:38	26:59:57
BayesTyper	19:15:14	21:06:09	23:30:17	27:47:37
bwa + Platypus	20:24:03	39:20:30	76:55:22	115:32:52
bwa + GATK ¹	47:24:18	74:16:30	125:25:19	177:37:56
bwa + Paragraph ²	21:49:04	42:42:03	84:28:32	127:27:47

¹ GATK was run on SNPs, small and midsize variants only.

² Paragraph was run on midsize and large variants only.

Table 1: **Runtimes** (in CPU hhh:mm:ss) for sample **HG00731** on all coverage levels. Note that GATK was only run on SNPs, small and midsize variants. Paragraph was only run on midsize and large variants. All other methods were run on all variant types.

213

214 2.4 Genotyping larger cohorts

215 The low runtime of PanGenie makes it well suited to genotype large cohorts. To demonstrate this use case, we applied
216 our tool to a set of 100 randomly selected 1000 Genomes samples based on 1000 Genomes Project high-coverage data
217 (Mike Zody, personal communication). We genotyped all variants contained in the callset that we described in section
218 2.2 and the 2×11 haplotypes contained in our extended panel. We used VCFTools [44] to test the genotype predictions
219 of bi-allelic variants for conformance with Hardy-Weinberg equilibrium and corrected for multiple hypothesis testing
220 by applying Benjamini-Hochberg correction [45] ($\alpha = 0.05$). We skipped such variant positions at which there was a
221 missing genotype for more than 10 samples.

222 We observed no significant deviation from Hardy-Weinberg equilibrium for 95.7% of all bi-allelic variants. When
223 looking at the different variant types individually, this percentage is between 93.7% and 95.7% (Figure 6), indicating that
224 the genotype predictions made by PanGenie are of good quality. Even for larger structural variants, allele frequencies
225 obtained from our variant predictions largely behave as expected by Hardy-Weinberg equilibrium (Figure 6). At the
226 same time, PanGenie on average only took about 30 CPU hours per sample, demonstrating the scalability of our tool.

227 3 Discussion

228 We presented an algorithm which uses k-mer counts from short read sequencing data together with a panel of haplotype-
229 resolved assemblies to genotype a yet uncharacterized sample. We show how to formulate this problem in terms of a
230 Hidden Markov Model that models each of the haplotypes of the sample in question as a mosaic of the given haplotype
231 sequences. This algorithm is fast since it bypasses the expensive read alignment step and can also genotype variants
232 located in repetitive or duplicated regions of the genome that are usually poorly covered by unique k-mers. We believe
233 that this is the first approach which can leverage the long-range haplotype information inherent to a panel of assembled
234 haplotype sequences in combination with read k-mer counts for genotyping a new sample. While we generated such
235 pangenome reference panels from haplotype-resolved assemblies for this work, we want to stress that generating these
236 panels was not the main focus of this paper and that our genotyping algorithm is not restricted to panels created in this
237 way. In fact, it can be applied to any acyclic pangenome graph which is represented as a fully-phased, multisample
238 VCF file.

239 Our experiments showed that PanGenie works as well as mapping-based approaches for small variants, and at the
240 same time, was able to genotype larger fractions of variants compared to the other k-mer based method BayesTyper.
241 Especially for large and midsize variants, PanGenie clearly outperforms mapping-based approaches, while again,

variant type	total	no sign. deviation from HWE
SNPs	5869317	5575453 (95.0%)
small insertions	412565	385735 (93.5%)
small deletions	426820	402421 (94.3%)
midsize insertions	12059	11139 (92.4%)
midsize deletions	8736	8200 (93.9%)
large insertions	8268	7536 (91.1%)
large deletions	3519	3249 (92.3%)
all	6741284	6393733 (94.8%)

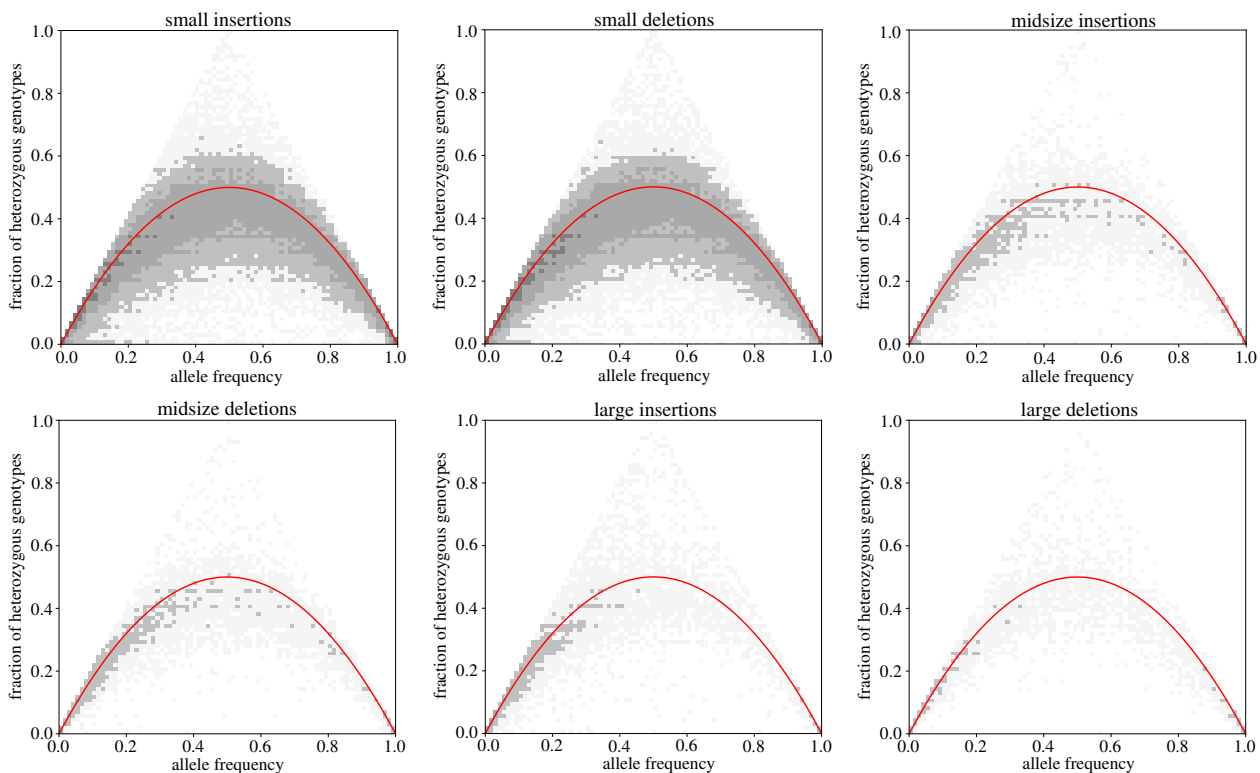
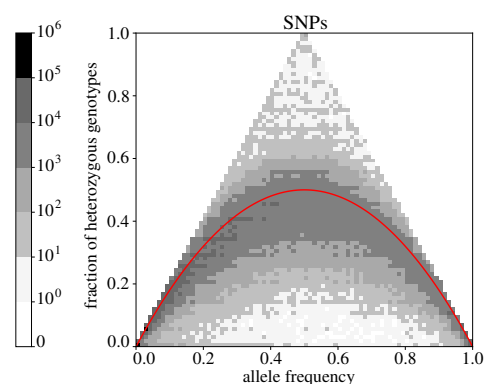


Figure 6: **Genotyping larger cohorts.** The table provides the amount of variants for which no significant deviation from Hardy-Weinberg Equilibrium was observed. Each plot shows the fraction of heterozygous genotypes at a variant position as a function of the allele frequency. The red curve shows what is expected according to Hardy-Weinberg equilibrium.

242 compared to BayesTyper, being able to provide genotypes for much larger amounts of variants not typable by the latter.
 243 At the same time, our approach was faster than the other methods, especially when comparing to the mapping-based
 244 approaches which require alignments of reads to a reference genome. The fast runtime of our method also makes it well
 245 suited for genotyping larger cohorts.

246 We hence have presented a method that is both scalable and leverages a haplotype-resolved pangenome reference to
 247 enable genotyping of otherwise inaccessible variants. Still, some limitations remain. Since we assume that the unknown
 248 haplotypes of the sample to be genotyped are mosaics of the given panel haplotypes, it currently cannot be used in
 249 order to genotype rare variants that are only present in the sample, but in none of the other haplotypes. Here, we believe
 250 that there are exciting opportunities to define downstream workflow that only discover variation that our approach has
 251 not captured because it was not present in the reference panel. That is, one could filter the reads for yet “unexplained”
 252 k-mers and use those for the discovery of rare variants.

253 The runtime of our method depends on the number of input haplotypes, as we define a hidden state for each possible
254 pair of haplotypes that can be selected at a variant position. Therefore, additional engineering will be required to use
255 much larger panels, which could be approached similarly to how statistical phasing packages prune the solution space
256 and/or proceed iteratively.

257 All in all, we have presented a method that we see as a way forward once high-quality phased reference assemblies
258 become widely available to the genomics community while, at the same time, the size of disease cohort used in
259 association studies grows further.

260 4 Methods

261 The input to our genotyping algorithm is a reference genome (FASTA-file), short-read sequencing reads (FASTQ
262 format) and a multisample VCF file that defines a pangenome graph containing variants and known haplotype sequences.
263 In order to create such an input VCF, we have developed a pipeline which calls variants from haplotype resolved
264 assemblies as described below. However, we want to stress that our tool is not restricted to VCFs created in this way
265 and in fact can be run with any fully phased, multisample VCF file.

266 4.1 Pangenome reference construction

267 We used haplotype-resolved assemblies of five individuals (HG00731, HG00732, NA12878, NA24385 and PGP1)
268 [34, 35] and separately aligned the contigs of each haplotype to the reference genome (GRCh38). This was done using
269 minimap2 [46] with parameters `-cx asm5 --cs`. Next, we called variants on each haplotype using paftools (<https://github.com/lh3/minimap2/tree/master/misc>) with default parameters. We only kept variants located in
270 regions in which all haplotypes were covered by exactly one contig alignment in order to filter out low quality or
271 erroneous calls. All other regions, in which at least one of the haplotypes was covered by none or multiple contig
272 alignments, were excluded from further analyses.

274 Our goal is to construct an acyclic and directed graph by inserting the variants of all haplotypes into the linear reference
275 genome. Each variant produces a bubble in the graph whose branches define the corresponding alleles. The input
276 haplotypes can be represented as paths through the resulting pangenome. When constructing the graph, we represent
277 sets of variants overlapping across haplotypes as a single bubble with potentially multiple branches reflecting all the
278 allele sequences observed in the haplotypes in the respective genomic region. See Figure 2 for an example. We represent
279 the pangenome in terms of a fully phased, multi-sample VCF file that contains an entry for each bubble in the graph. At
280 each site, the number of alternative alleles is limited by the number of input haplotype sequences and the genotypes of
281 each sample define two paths through this graph corresponding to the respective haplotypes.

282 We extended the number of haplotype paths in the graph by using PanGenie to phase additional samples based on short
283 read sequencing data and the paths already present in our graph. This is achieved by applying the Viterbi algorithm to
284 our Hidden Markov Model (see Section 4.3 for details). In this way, we added haplotypes of six additional individuals
285 to the graph. These include samples of Chinese and Yorubian descent (HG00512, NA19238) as well as four samples
286 from different populations (see Figure 3a) The underlying reads for the Chinese and Yorubian samples were obtained
287 from [3] and those of the remaining samples from 1000 Genomes Project high-coverage data (Mike Zody, personal
288 communication). We used bcftools (<https://github.com/samtools/bcftools>), VCFTools [44] and vcfstats
289 from Real Time Genomics [47] to generate the callset statistics presented in Figure 3.

290 The individuals of Puerto Rican, Chinese and Yorubian descent, are part of three trios. We additionally determined the
291 genotypes for the remaining samples (HG00733, HG00513 and HG00514, NA19239 and NA19240). This was done in
292 a similar way as for the other samples, using haplotype-resolved assemblies to determine phasings for HG00733, and
293 short-read sequencing reads in order to phase the remaining samples, for which such assemblies were not available
294 to us. Using the trio information, we can check whether the variant calls are consistent with the laws of Mendelian
295 inheritance. For the Puerto Rican trio, we observed 98.34% Mendelian consistent genotypes for the phasings produced
296 from haplotype-resolved assemblies. For the Chinese and Yorubian trios, these percentages were 98.76% and 97.96%,
297 respectively, for the phasings produced by PanGenie. For further analysis, we removed all variants from our graph for
298 which there was a Mendelian error in at least one of the trios.

299 4.2 Identifying unique k-mers

300 Sets of variants that are less than the k-mer size apart (we use $k = 31$) are combined and treated as a single variant
301 position. The alleles corresponding to such a combined variant are defined by the haplotype paths in the respective
302 region. For each variant position v , we determine a set of k-mers, $kmers_v$, that uniquely characterize the variant

303 region. This is done by counting all k-mers along haplotype paths in the pangenome graph using Jellyfish [36], and
 304 then determining a set of k-mers for each variant, that occur at most once within a single allele sequence and are not
 305 found anywhere outside of the variant bubble. We additionally count all k-mers of the graph in the sequencing reads.

306 **4.3 Hidden Markov Model**

307 We define a Hidden Markov Model that can be used to compute the two most likely haplotype sequences of a given
 308 sample based on known haplotype paths and the sample reads. The new haplotype sequences are combinations of
 309 the existing paths through the graph and are computed based on the copy numbers of unique k-mers observed in the
 310 sequencing reads provided for the sample to be genotyped.

Hidden States and Transitions. We assume to be given N haplotype paths $H_i, i = 1, \dots, N$, through the graph. Furthermore, for each variant position $v, v = 1, \dots, M$, we are given a vector of k-mers, $kmers_v$ that uniquely characterize the alleles of a variant. We assume some (arbitrary) order of the elements in $kmers_v$ and refer to the i th k-mer as $kmers_v[i]$. Additionally, we are given sequencing data of the sample to be genotyped and corresponding k-mer counts for all k-mers in $kmers_v$. For each variant position v , we define set of hidden states $\mathcal{H}_v = \{H_{v,i,j} \mid i, j \leq N\}$ which contains a state for each possible pair of the N given haplotype paths in the graph. Each such state $H_{v,i,j}$ induces an assignment of copy numbers to all k-mers in $kmers_v$ defined as shown below.

$$cn(k, i, j) = \begin{cases} 0 & k \notin H_i \cup H_j \\ 1 & k \in H_i \setminus H_j \\ 1 & k \in H_j \setminus H_i \\ 2 & k \in H_i \cap H_j \end{cases} \quad \forall k \in kmers_v, i, j = 1, \dots, N$$

311 The idea here is that we expect to see copy number 2 for all k-mers occurring on both haplotype paths. In case only one
 312 of the haplotypes contains a k-mer, its copy number must be 1 and k-mers that do not appear in any of the two paths
 313 must have copy number 0. Thus, for each state $H_{v,i,j}$ in \mathcal{H}_v , we define the vector $a_{v,i,j}$ that contains the assigned copy
 314 numbers for all k-mers, i.e. $a_{v,i,j}[l] = cn(kmers_v[l], i, j)$.

315 From each state $H_{v,i,j} \in \mathcal{H}_v$ that corresponds to variant position v , there is a transition to each state corresponding to
 316 the next position, $v + 1$. Additionally, there is a *start* state, from which there is a transition to each state of the first
 317 variant, and an *end* state, to which there is a transition from each state that corresponds to the last variant position. See
 318 Figure 1c for an example.

319 **Transition Probabilities.** Transition probabilities are computed similar to how the Li-Stephans model [28] defines
 320 them. We assume to be given a recombination rate r and the effective population size N_e . For two ascending variant
 321 positions $v - 1$ and v that are x bases apart in the genome, we first compute the genetic distance:

$$d = x \cdot \frac{1}{1000000} \cdot r \cdot 4 \cdot N_e$$

We further compute the Li-Stephans transition probabilities as:

$$p_r = (1 - \exp(-\frac{d}{N})) \cdot \frac{1}{N}$$

$$q_r = \exp(-\frac{d}{N}) + p_r$$

322 Finally, the transition probability from state $H_{v-1,i,j}$ to state $H_{v,k,l}$ is computed as shown below.

$$P(H_{v,i,j} | H_{v-1,k,l}) = \begin{cases} q_r \cdot q_r & i = k \text{ and } j = l \\ q_r \cdot p_r & i = k \text{ and } j \neq l \\ q_r \cdot p_r & i \neq k \text{ and } j = l \\ p_r \cdot p_r & i \neq k \text{ and } j \neq l \end{cases} \quad (2)$$

Observable States. Each hidden state $H_{v,i,j} \in \mathcal{H}_v$ outputs a count for each k-mer in $kmers_v$. Let $obs(k)$ be a function that returns the observed count in the reads of a k-mer $k \in \mathcal{K}$ and the vector such that $\mathcal{O}_v[l] = obs(kmers_v[l])$. In order to define the emission probabilities, we first need to model the distribution of k-mer counts for each copy number, $P(obs(k) | cn(k) = i), i = 0, 1, 2$. For copy number 2, we use a Poisson distribution whose mean λ we compute from the read k-mer-count histogram. Similarly, we approximate the k-mer count distribution for copy number

1 in terms of a Poisson distribution with mean $\lambda/2$. For copy number 0, we need to model the erroneous k-mers that arise from sequencing errors. This is done using a Geometric distribution, whose parameter p we choose based on the mean k-mer coverage. Finally, we compute the emission probability for a given state and given observed read k-mer counts as shown below, making the assumption that the k-mer counts are independent.

$$P(\mathcal{O}_v | H_{v,i,j}) = \prod_{l=1}^{|kmer_{v,i,j}|} P(\mathcal{O}_v[l] | a_{v,i,j}[l])$$

323 **Genotypes and Haplotypes.** In this model, genotypes correspond to pairs of given haplotype paths at each variant
 324 position. Genotype likelihoods can be computed using the Forward-Backward algorithm, and haplotype sequences can
 325 be computed by running Viterbi. We assume to have observed copy number $obs(k)$ of each unique k-mers in \mathcal{K} .

Forward-Backward algorithm. The initial distribution of our HMM is such that we assign probability 1 in the *start* state and 0 to all others. Forward probabilities $\alpha_v()$ are computed in the following way.

$$\alpha_0(start) = 1$$

For states corresponding to variant position $v = 1, \dots, M$, the Forward probabilities are computed as shown below. The set of observed k-mer counts at position v is given by $\mathcal{O}_v = \{obs(k), k \in kmer_{v,i,j}\}$.

$$\alpha_v(H_{v,i,j}) = \sum_{H_{v-1,s,t} \in \mathcal{H}_{v-1}} \alpha_{v-1}(H_{v-1,s,t}) \cdot P(H_{v,i,j} | H_{v-1,s,t}) \cdot P(\mathcal{O}_v | H_{v,i,j}) \quad \forall i, j$$

The transition probabilities are computed as described above, except for transitions from the *start* state to all states in the first column, which we assume to have uniform probabilities.

Backward probabilities are computed in a similar manner. We set

$$\beta_M(end) = 1$$

For $v = 1, \dots, M-1$, we compute them as

$$\beta_v(H_{v,i,j}) = \sum_{H_{v+1,s,t} \in \mathcal{H}_{v+1}} \beta_{v+1}(H_{v+1,s,t}) \cdot P(H_{v+1,s,t} | H_{v,i,j}) \cdot P(\mathcal{O}_v | H_{v+1,s,t}) \quad \forall i, j$$

326 Finally, posterior probabilities for the states can be computed.

$$P(H_{v,i,j} | \mathcal{O}) = \frac{\alpha_v(H_{v,i,j}) \cdot \beta_v(H_{v,i,j})}{\sum_{h \in \mathcal{H}_v} \alpha_v(h) \beta_v(h)}$$

327 Several states at a variant position v can correspond to the same genotype, as different paths can cover the same allele.
 328 Also, the alleles in a genotype are unordered, therefore states $H_{v,i,j}$ and $H_{v,j,i}$ always lead to the same genotype. In
 329 order to compute genotype likelihoods, we sum up the posterior probabilities for all states that correspond to the same
 330 genotype. In this way, we can finally compute genotype likelihoods for all genotypes at a variant position, based on
 331 which a genotype prediction can be made.

Viterbi algorithm. In order to get the haplotype sequences, we can compute the two haplotypes underlying the Viterbi path. We again start in the *start* state.

$$v_0(start) = 1$$

For the other positions $v = 1, \dots, M$, we compute:

$$v_v(H_{v,i,j}) = \max_{H_{v-1,s,t} \in \mathcal{H}_{v-1}} \alpha_{v-1}(H_{v-1,s,t}) \cdot P(H_{v,i,j} | H_{v-1,s,t}) \cdot P(\mathcal{O}_v | H_{v,i,j}) \quad \forall i, j$$

332 We finally obtain the Viterbi path by backtracking.

333 Availability of data and materials

334 Code to reproduce the data and rerun the analysis is available at https://bitbucket.org/jana_ebler/genotyping-experiments/src/master/.

336 The implementation of PanGenie is available at https://bitbucket.org/jana_ebler/pangenie/src/master/.

337 **References**

338 [1] 1000 Genomes Project Consortium et al. A global reference for human genetic variation. *Nature*, 526(7571):68, 339 2015.

340 [2] Peter H Sudmant, Tobias Rausch, Eugene J Gardner, Robert E Handsaker, Alexej Abyzov, John Huddleston, Yan 341 Zhang, Kai Ye, Goo Jun, Markus Hsi-Yang Fritz, et al. An integrated map of structural variation in 2,504 human 342 genomes. *Nature*, 526(7571):75, 2015.

343 [3] Mark JP Chaisson, Ashley D Sanders, Xuefang Zhao, Ankit Malhotra, David Porubsky, Tobias Rausch, Eugene J 344 Gardner, Oscar L Rodriguez, Li Guo, Ryan L Collins, et al. Multi-platform discovery of haplotype-resolved 345 structural variation in human genomes. *Nature communications*, 10, 2019.

346 [4] Ryan L Collins, Harrison Brand, Konrad J Karczewski, Xuefang Zhao, Jessica Alföldi, Laurent C Francioli, 347 Amit V Khera, Chelsea Lowther, Laura D Gauthier, Harold Wang, et al. A structural variation reference for 348 medical and population genetics. *Nature*, 581(7809):444–451, 2020.

349 [5] Nick Craddock, Matthew E Hurles, Niall Cardin, Richard D Pearson, Vincent Plagnol, Samuel Robson, Damjan 350 Vukcevic, Chris Barnes, Donald F Conrad, Eleni Giannoulatou, et al. Genome-wide association study of cnvs in 351 16,000 cases of eight common diseases and 3,000 shared controls. *Nature*, 464(7289):713, 2010.

352 [6] Nigel M Williams, Irina Zaharieva, Andrew Martin, Kate Langley, Kiran Mantripragada, Ragnheiður Fossdal, 353 Hreinn Stefansson, Kari Stefansson, Pall Magnusson, Olafur O Gudmundsson, et al. Rare chromosomal deletions 354 and duplications in attention-deficit hyperactivity disorder: a genome-wide analysis. *The Lancet*, 376(9750):1401– 355 1408, 2010.

356 [7] Jonathan Sebat, B Lakshmi, Dheeraj Malhotra, Jennifer Troge, Christa Lese-Martin, Tom Walsh, Boris Yamrom, 357 Seungtai Yoon, Alex Krasnitz, Jude Kendall, et al. Strong association of de novo copy number mutations with 358 autism. *Science*, 316(5823):445–449, 2007.

359 [8] Stephan J Sanders, A Gulhan Ercan-Sençicek, Vanessa Hus, Rui Luo, Michael T Murtha, Daniel Moreno-De-Luca, 360 Su H Chu, Michael P Moreau, Abha R Gupta, Susanne A Thomson, et al. Multiple recurrent de novo cnvs, 361 including duplications of the 7q11.23 williams syndrome region, are strongly associated with autism. *Neuron*, 362 70(5):863–885, 2011.

363 [9] Dheeraj Malhotra, Shane McCarthy, Jacob J Michaelson, Vladimir Vacic, Katherine E Burdick, Seungtai Yoon, 364 Sven Cichon, Aiden Corvin, Sydney Gary, Elliot S Gershon, et al. High frequencies of de novo cnvs in bipolar 365 disorder and schizophrenia. *Neuron*, 72(6):951–963, 2011.

366 [10] Tom Walsh, Jon M McClellan, Shane E McCarthy, Anjené M Addington, Sarah B Pierce, Greg M Cooper, Alex S 367 Nord, Mary Kusenda, Dheeraj Malhotra, Abhishek Bhandari, et al. Rare structural variants disrupt multiple genes 368 in neurodevelopmental pathways in schizophrenia. *science*, 320(5875):539–543, 2008.

369 [11] Mark A DePristo, Eric Banks, Ryan Poplin, Kiran V Garimella, Jared R Maguire, Christopher Hartl, Anthony A 370 Philippakis, Guillermo Del Angel, Manuel A Rivas, Matt Hanna, et al. A framework for variation discovery and 371 genotyping using next-generation dna sequencing data. *Nature genetics*, 43(5):491, 2011.

372 [12] Erik Garrison and Gabor Marth. Haplotype-based variant detection from short-read sequencing. *arXiv preprint 373 arXiv:1207.3907*, 2012.

374 [13] Tobias Rausch, Thomas Zichner, Andreas Schlattl, Adrian M Stütz, Vladimir Benes, and Jan O Korbel. Delly: 375 structural variant discovery by integrated paired-end and split-read analysis. *Bioinformatics*, 28(18):i333–i339, 376 2012.

377 [14] Andy Rimmer, Hang Phan, Iain Mathieson, Zamin Iqbal, Stephen RF Twigg, Andrew OM Wilkie, Gil McVean, 378 Gerton Lunter, WGS500 Consortium, et al. Integrating mapping-, assembly-and haplotype-based approaches for 379 calling variants in clinical sequencing applications. *Nature genetics*, 46(8):912, 2014.

380 [15] Colby Chiang, Ryan M Layer, Gregory G Faust, Michael R Lindberg, David B Rose, Erik P Garrison, Gabor T 381 Marth, Aaron R Quinlan, and Ira M Hall. Speedseq: ultra-fast personal genome analysis and interpretation. *Nature 382 methods*, 12(10):966, 2015.

383 [16] Erik Garrison, Jouni Sirén, Adam M Novak, Glenn Hickey, Jordan M Eizenga, Eric T Dawson, William Jones, 384 Shilpa Garg, Charles Markello, Michael F Lin, et al. Variation graph toolkit improves read mapping by representing 385 genetic variation in the reference. *Nature biotechnology*, 36(9):875–879, 2018.

386 [17] Goran Rakocovic, Vladimir Semenyuk, Wan-Ping Lee, James Spencer, John Browning, Ivan J Johnson, Vladan 387 Arsenijevic, Jelena Nadj, Kaushik Ghose, Maria C Suciu, et al. Fast and accurate genomic analyses using genome 388 graphs. *Nature genetics*, 51(2):354–362, 2019.

389 [18] Hannes P Eggertsson, Hakon Jonsson, Snaedis Kristmundsdottir, Eirikur Hjartarson, Birte Kehr, Gisli Masson, 390 Florian Zink, Kristjan E Hjorleifsson, Aslaug Jonasdottir, Adalbjorg Jonasdottir, et al. Graphyper enables 391 population-scale genotyping using pangenome graphs. *Nature genetics*, 49(11):1654, 2017.

392 [19] Daehwan Kim, Joseph M Paggi, Chanhee Park, Christopher Bennett, and Steven L Salzberg. Graph-based genome 393 alignment and genotyping with hisat2 and hisat-genotype. *Nature biotechnology*, 37(8):907–915, 2019.

394 [20] Sai Chen, Peter Krusche, Egor Dolzhenko, Rachel M Sherman, Roman Petrovski, Felix Schlesinger, Melanie 395 Kirsche, David R Bentley, Michael C Schatz, Fritz J Sedlazeck, and Michael A Eberle. Paragraph: A graph-based 396 structural variant genotyper for short-read sequence data. *Genome Biology*, 20:201, 2019.

397 [21] Glenn Hickey, David Heller, Jean Monlong, Jonas Andreas Sibbesen, Jouni Siren, Jordan Eizenga, Eric Dawson, 398 Erik Garrison, Adam Novak, and Benedict Paten. Genotyping structural variants in pangenome graphs using the 399 vg toolkit. *BioRxiv*, page 654566, 2019.

400 [22] Zamin Iqbal, Mario Caccamo, Isaac Turner, Paul Flicek, and Gil McVean. De novo assembly and genotyping of 401 variants using colored de bruijn graphs. *Nature genetics*, 44(2):226, 2012.

402 [23] Alexander Dilthey, Charles Cox, Zamin Iqbal, Matthew R Nelson, and Gil McVean. Improved genome inference 403 in the mhc using a population reference graph. *Nature genetics*, 47(6):682, 2015.

404 [24] Dirk D Dolle, Zhicheng Liu, Matthew Cotten, Jared T Simpson, Zamin Iqbal, Richard Durbin, Shane A McCarthy, 405 and Thomas M Keane. Using reference-free compressed data structures to analyze sequencing reads from 406 thousands of human genomes. *Genome research*, 27(2):300–309, 2017.

407 [25] Jonas Andreas Sibbesen, Lasse Maretty, and Anders Krogh. Accurate genotyping across variant classes and 408 lengths using variant graphs. *Nature genetics*, 50(7):1054, 2018.

409 [26] Joachim Weischenfeldt, Orsolya Symmons, Francois Spitz, and Jan O Korbel. Phenotypic impact of genomic 410 structural variation: insights from and for human disease. *Nature Reviews Genetics*, 14(2):125, 2013.

411 [27] Isaac Turner, Kiran V Garimella, Zamin Iqbal, and Gil McVean. Integrating long-range connectivity information 412 into de bruijn graphs. *Bioinformatics*, 34(15):2556–2565, 2018.

413 [28] Na Li and Matthew Stephens. Modeling linkage disequilibrium and identifying recombination hotspots using 414 single-nucleotide polymorphism data. *Genetics*, 165(4):2213–2233, 2003.

415 [29] Bryan Howie, Jonathan Marchini, and Matthew Stephens. Genotype imputation with thousands of genomes. *G3: 416 Genes, Genomes, Genetics*, 1(6):457–470, 2011.

417 [30] Androniki Menelaou and Jonathan Marchini. Genotype calling and phasing using next-generation sequencing 418 reads and a haplotype scaffold. *Bioinformatics*, 29(1):84–91, January 2013.

419 [31] Sayantan Das, Lukas Forer, Sebastian Schönherr, Carlo Sidore, Adam E Locke, Alan Kwong, Scott I Vrieze, 420 Emily Y Chew, Shawn Levy, Matt McGuire, et al. Next-generation genotype imputation service and methods. 421 *Nature genetics*, 48(10):1284–1287, 2016.

422 [32] Brian L Browning and Sharon R Browning. Genotype imputation with millions of reference samples. *The 423 American Journal of Human Genetics*, 98(1):116–126, 2016.

424 [33] Sergey Koren, Arang Rhee, Brian P Walenz, Alexander T Dilthey, Derek M Bickhart, Sarah B Kingan, Stefan 425 Hiendleder, John L Williams, Timothy P L Smith, and Adam M Phillippy. De novo assembly of haplotype-resolved 426 genomes with trio binning. *Nat. Biotechnol.*, October 2018.

427 [34] Shilpa Garg, Arkarachai Arkarachai Fungtammasan, Andrew Carroll, Mike Chou, Anthony Schmitt, Xiang Zhou, 428 Stephen Mac, Paul Peluso, Emily Hatas, Jay Ghurye, et al. Efficient chromosome-scale haplotype-resolved 429 assembly of human genomes. *BioRxiv*, page 810341, 2019.

430 [35] David Porubsky, Peter Ebert, Peter A Audano, Mitchell R Vollger, William T Harvey, Katherine M Munson, 431 Melanie Sorensen, Arvis Sulovari, Marina Haukness, Maryam Ghareghani, et al. A fully phased accurate assembly 432 of an individual human genome. *BioRxiv*, page 855049, 2019.

433 [36] Guillaume Marçais and Carl Kingsford. A fast, lock-free approach for efficient parallel counting of occurrences of 434 k-mers. *Bioinformatics*, 27(6):764–770, 2011.

435 [37] Yan Guo, Fei Ye, Quanghu Sheng, Travis Clark, and David C Samuels. Three-stage quality control strategies for 436 dna re-sequencing data. *Briefings in bioinformatics*, 15(6):879–889, 2013.

437 [38] Jing Wang, Leon Raskin, David C Samuels, Yu Shyr, and Yan Guo. Genome measures used for quality control are 438 dependent on gene function and ancestry. *Bioinformatics*, 31(3):318–323, 2014.

439 [39] Jing Wang, David C Samuels, Yu Shyr, and Yan Guo. Population structure analysis on 2504 individuals across 26 440 ancestries using bioinformatics approaches. *BMC bioinformatics*, 16(15):P19, 2015.

441 [40] Justin M Zook, Nancy F Hansen, Nathan D Olson, Lesley M Chapman, James C Mullikin, Chunlin Xiao, Stephen
442 Sherry, Sergey Koren, Adam M Phillippy, Paul C Boutros, et al. A robust benchmark for germline structural
443 variant detection. *BioRxiv*, page 664623, 2019.

444 [41] Heng Li and Richard Durbin. Fast and accurate long-read alignment with burrows–wheeler transform. *Bioinformatics*, 26(5):589–595, 2010.

446 [42] Donna Karolchik, Angela S Hinrichs, Terrence S Furey, Krishna M Roskin, Charles W Sugnet, David Haussler,
447 and W James Kent. The ucsc table browser data retrieval tool. *Nucleic acids research*, 32(suppl_1):D493–D496,
448 2004.

449 [43] Justin M Zook, Jennifer McDaniel, Nathan D Olson, Justin Wagner, Hemang Parikh, Haynes Heaton, Sean A
450 Irvine, Len Trigg, Rebecca Truty, Cory Y McLean, et al. An open resource for accurately benchmarking small
451 variant and reference calls. *Nature biotechnology*, 37(5):561, 2019.

452 [44] Petr Danecek, Adam Auton, Goncalo Abecasis, Cornelis A Albers, Eric Banks, Mark A DePristo, Robert E
453 Handsaker, Gerton Lunter, Gabor T Marth, Stephen T Sherry, et al. The variant call format and vcftools.
454 *Bioinformatics*, 27(15):2156–2158, 2011.

455 [45] Yoav Benjamini and Yosef Hochberg. Controlling the false discovery rate: a practical and powerful approach to
456 multiple testing. *Journal of the Royal statistical society: series B (Methodological)*, 57(1):289–300, 1995.

457 [46] Heng Li. Minimap2: pairwise alignment for nucleotide sequences. *Bioinformatics*, 34(18):3094–3100, 2018.

458 [47] John G Cleary, Ross Braithwaite, Kurt Gaastra, Brian S Hilbush, Stuart Inglis, Sean A Irvine, Alan Jackson,
459 Richard Littin, Mehul Rathod, David Ware, et al. Comparing variant call files for performance benchmarking of
460 next-generation sequencing variant calling pipelines. *BioRxiv*, page 023754, 2015.

461 [48] Aaron R Quinlan. Bedtools: the swiss-army tool for genome feature analysis. *Current protocols in bioinformatics*,
462 47(1):11–12, 2014.

463 **Supplementary material**

464 **Callset statistics**

465 Table 2 shows the numbers of variants of each type that were present in the callset constructed from reference-resolved
466 assemblies. For each sample, we show the total number of variants present in at least one of its haplotypes, i.e. all
467 variants for which the sample has a genotype different from 0/0 (total), as well as the number of variants for which a
468 sample carried at least one allele not seen in any of the remaining samples (unique). All variants that are unique to a
469 sample will not be genotypable by our HMM based approach, since the assumption underlying our model is that the
470 unknown haplotypes can be constructed as a mosaic of the haplotypes already known. Thus, if the sample in question
471 carries an allele not seen before, it cannot be correctly genotyped with such a re-typing approach.

type	HG00731		HG00732		NA12878		NA24385		PGP1		total
	total	unique									
SNP	3373316	403185	3389303	439356	3325551	378925	3366074	417201	3318739	383258	6145661
small insertion	234440	28826	244847	39585	232557	29133	237708	36741	244933	43243	461260
small deletion	226717	28092	233600	35492	228234	30416	271670	68500	245842	47462	493717
small complex	203420	51015	205868	58164	200898	48802	217340	85518	204459	57751	260595
midsize insertion	5907	1223	6081	1420	5817	1221	5929	1248	5986	1319	13201
midsize deletion	4730	667	4707	698	4649	643	4757	714	4626	638	9129
midsize complex	20102	9251	20178	9690	20027	9314	20251	10143	20075	9634	23694
large insertion	3502	1021	3665	1179	3560	1025	3575	1072	3599	1072	9202
large deletion	2096	207	2159	233	2055	191	2148	231	2101	192	3577
large complex	10264	4012	10269	4350	10304	4089	10442	4627	10284	4203	12818

Table 2: **Variant statistics.** Total number of variants detected in each sample, as well as the number of variants for which a sample carried an allele not present in the other samples.

472 **Comparison to gnomAD** We compared the variant calls that we obtained from haplotype-resolved assemblies
473 of five individuals to the variants that are part of the Genome Aggregation Database (gnomAD) [4]. gnomAD
474 contains 433,371 structural variants collected across 14,891 genomes from different populations. Since gnomAD calls
475 were generated relative to reference genome version hg19, we used UCSC liftOver (<https://genome.ucsc.edu/cgi-bin/hgLiftOver>) to convert their coordinates to hg38. We compared the variants contained in gnomAD to our
476 assembly-based variant calls. We excluded variants genotyped with an allele frequency of 0.0 across all 100 genotyped
477 samples (Section 2.4). We determined all variants with a reciprocal overlap of at least 50% between the gnomAD
478 calls and our assembly-based callset (chromosomes 1-22) and found that both callsets had 6,398 variants in common.
479 368,530 variants were only contained in gnomAD and 21,370 were only in our assembly callset. 35.3% of the 6,398
480 variants in the intersection are located inside of STR/VNTR regions. For the variants contained only in our assembly
481 callset, this percentage is around 80%. We suspect that the reason these variants cannot be found in gnomAD might be
482 that such repetitive regions are not accessible by short read data used to produce the gnomAD variant calls. For each
483 variant in our assembly callset, we further computed the distance to the closest gnomAD variant. Additionally, we used
484 bedtools shuffle [48] to randomly permute the variants among the genome. Then we again determined distances to
485 the closest gnomAD variants. We show the resulting distances in Figure 7.

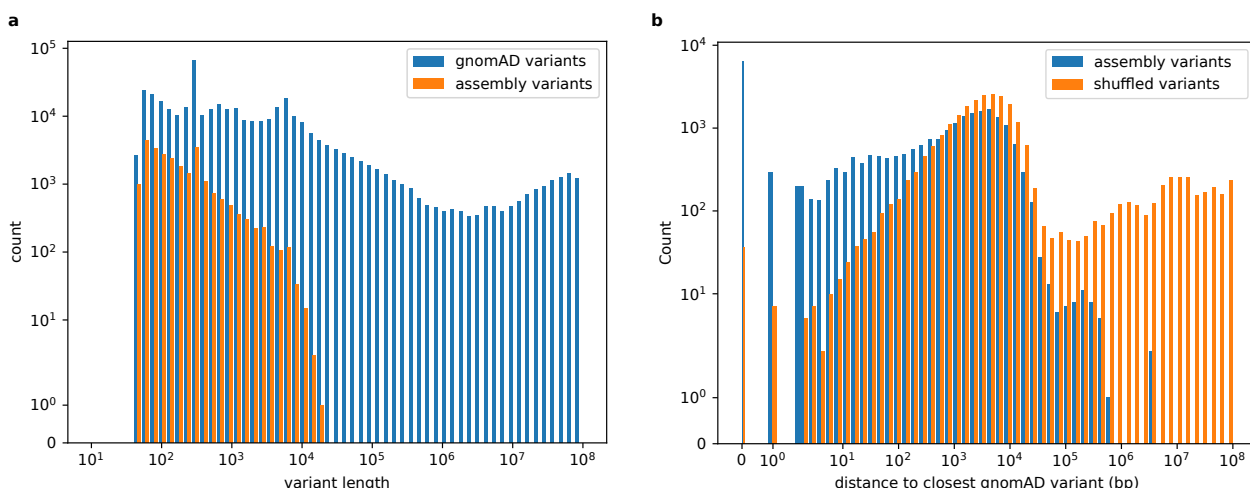


Figure 7: **Comparison to gnomAD.** a) Histogram of the variant length of the structural variants contained in the gnomAD callset (blue) and our assembly callset (orange). b) For each variant in our assembly callset, we computed the distance to the closest gnomAD variant (blue). We repeated the same analysis after randomly permuting our variant calls along the reference genome (orange).

487 Benchmarking results

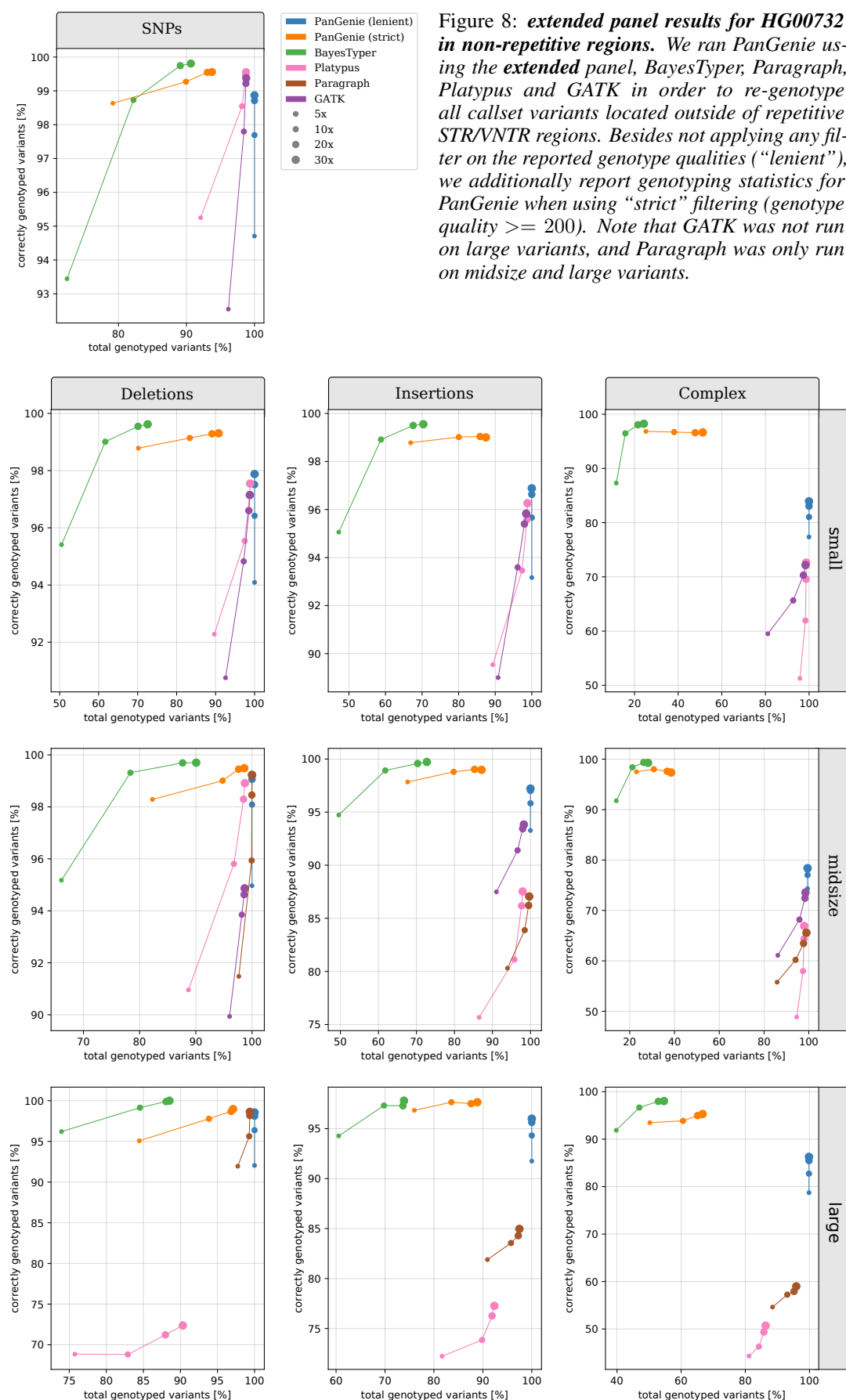
488 **STR/VNTR regions** Especially structural variants tend to be located in repetitive and more complicated regions of
489 the genome. For all variants that we genotyped in sample HG00731 (Section 2.3), we show the number of sites located
490 inside and outside of STR/VNTR regions which we obtained from the UCSC genome browser [42]. The numbers are
491 presented in Table 3. It can be observed that the majority (between 54 – 79%) of midsize and large variants are indeed
492 inside of repetitive regions.

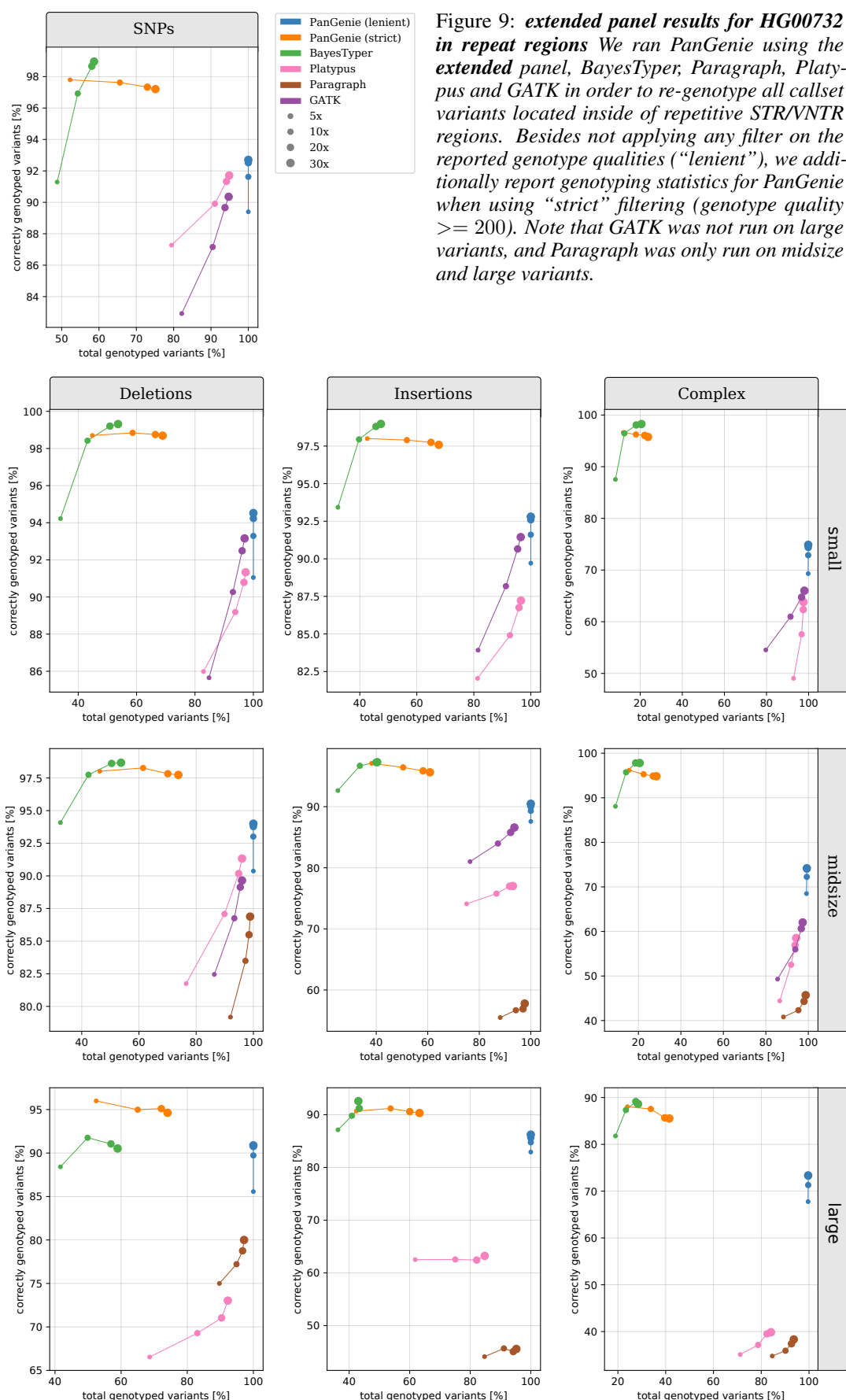
variant type	all regions	non-repetitive regions	repeat regions	
SNP	5742475	5527879	96,26%	214596 3,74%
small deletion	465625	401391	86,20%	64234 13,80%
small insertion	432434	382244	88,39%	50190 11,61%
small complex	209580	144809	69,09%	64771 30,91%
midsize deletion	8462	2971	35,11%	5491 64,89%
midsize insertion	11978	5497	45,89%	6481 54,11%
midsize complex	14443	3092	21,41%	11351 78,59%
large deletion	3370	1100	32,64%	2270 67,36%
large insertion	8178	3220	39,37%	4958 60,63%
large complex	8806	2071	23,52%	6735 76,48%

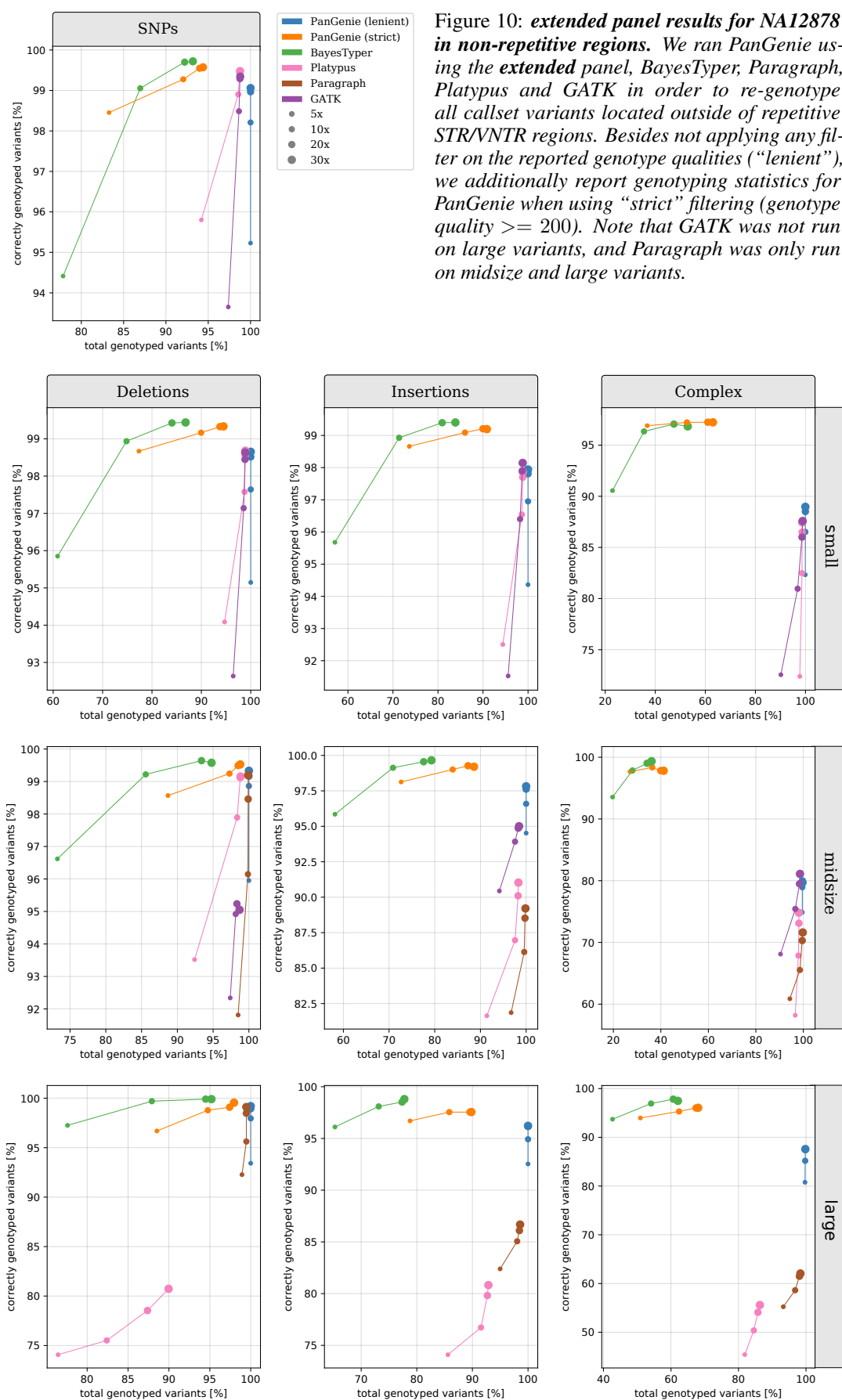
Table 3: **Repetitive regions.** Shown are the number and percentages of variants located inside and outside of STR/VNTR regions for sample HG00731.

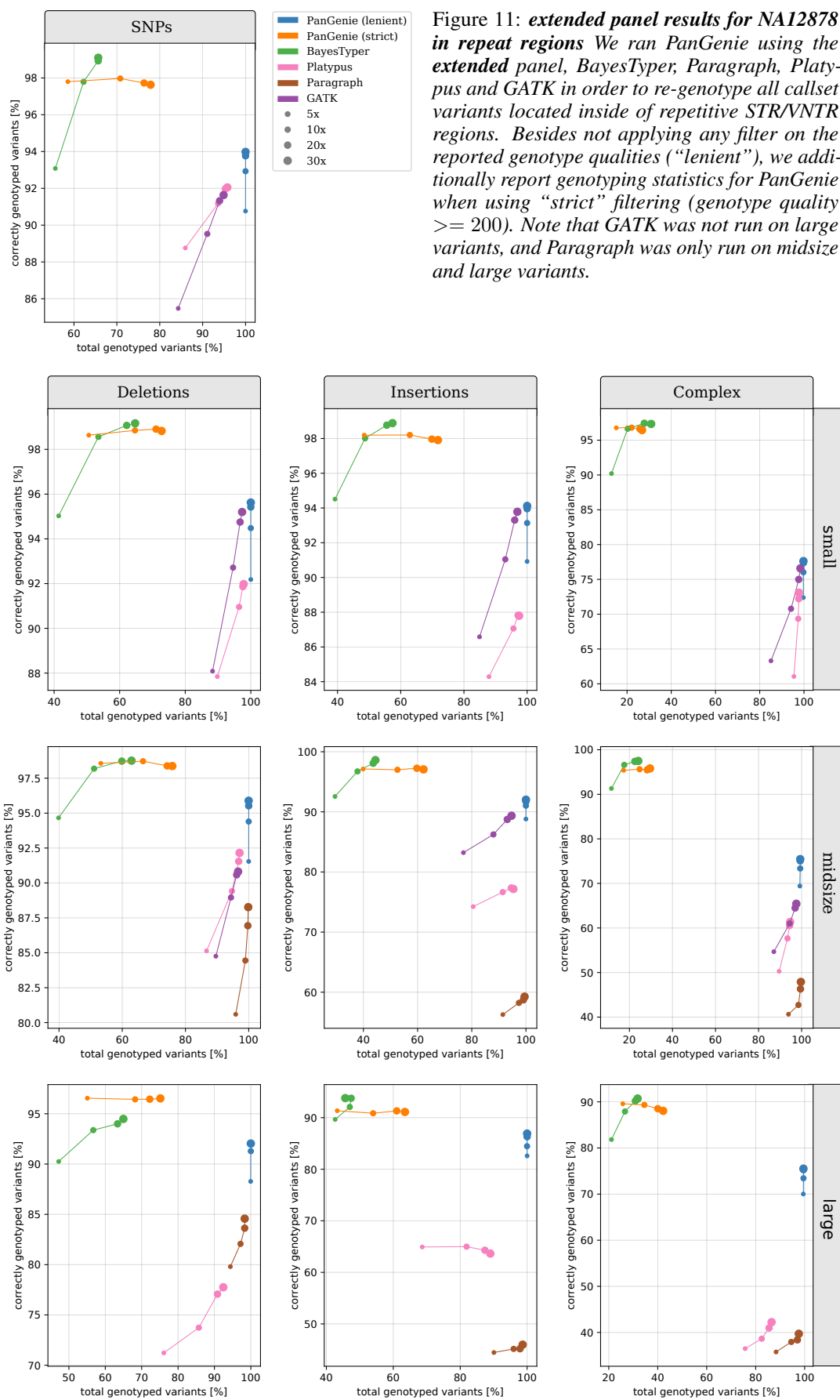
493 **Results for the extended panel** We additionally show the genotyping results of all methods using the extended panel
494 for samples HG00732, NA12878 and NA24385 in Figures 8-13. Genotyping experiments were run in the same way
495 as for HG00731 presented in Section 2.3. For PanGenie, we used the extended panel that contained 10 samples (20
496 haplotypes). Besides using all output genotypes produced by PanGenie regardless of the reported genotype quality
497 (“lenient”), we additionally report results of PanGenie when applying a much more strict filtering using genotype
498 quality score of 200 (“strict”). For all other tools, we used all genotypes that they reported and did not use any filtering
499 on genotype qualities. We again show results for variants inside and outside of repetitive regions.

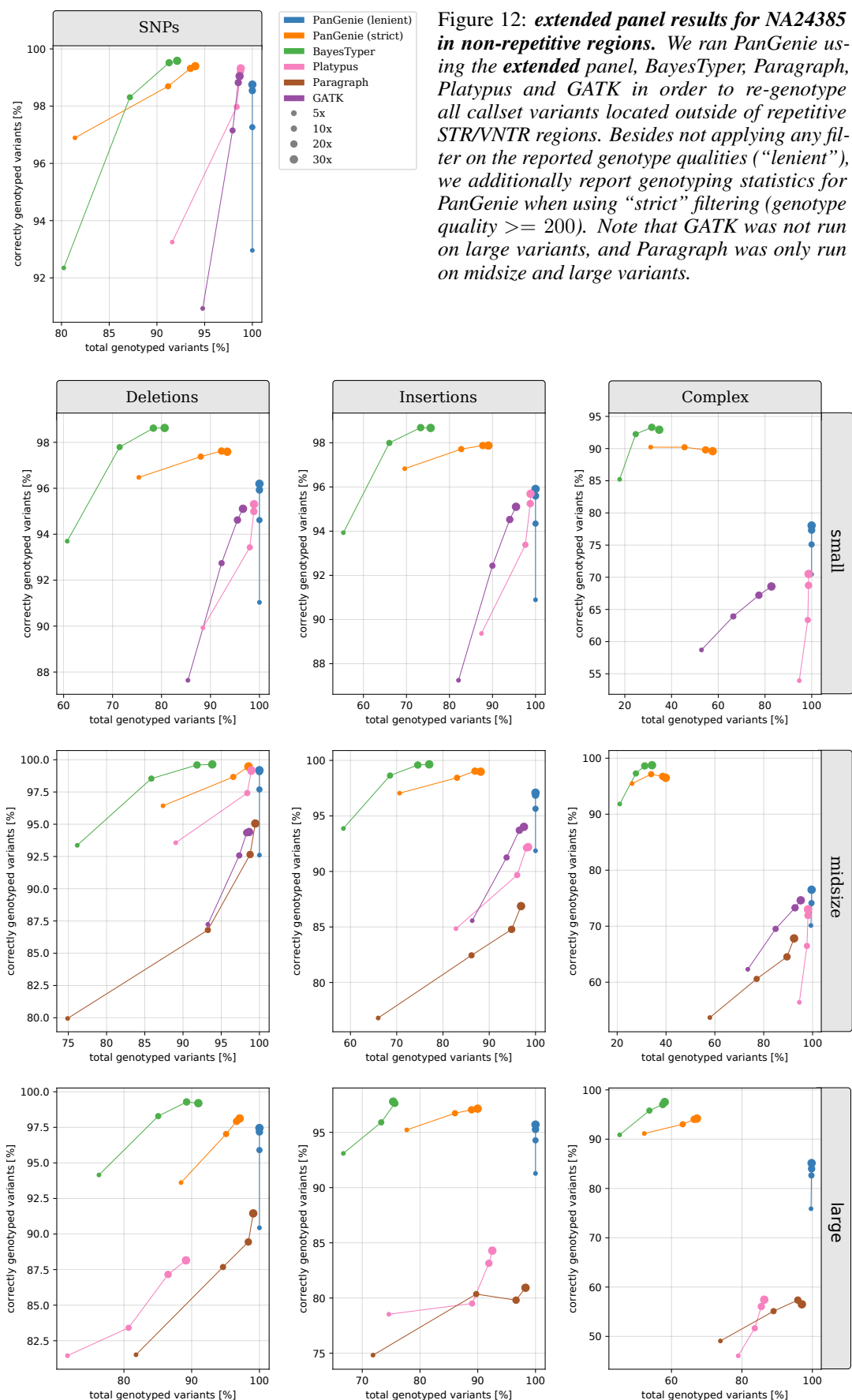
500 **Results for the small panel** We provide the genotyping results that we obtained for all four samples using the small
501 panel (8 haplotypes) in Figures 14-21. Experiments were run analogously to what we describe in Section 2.3.

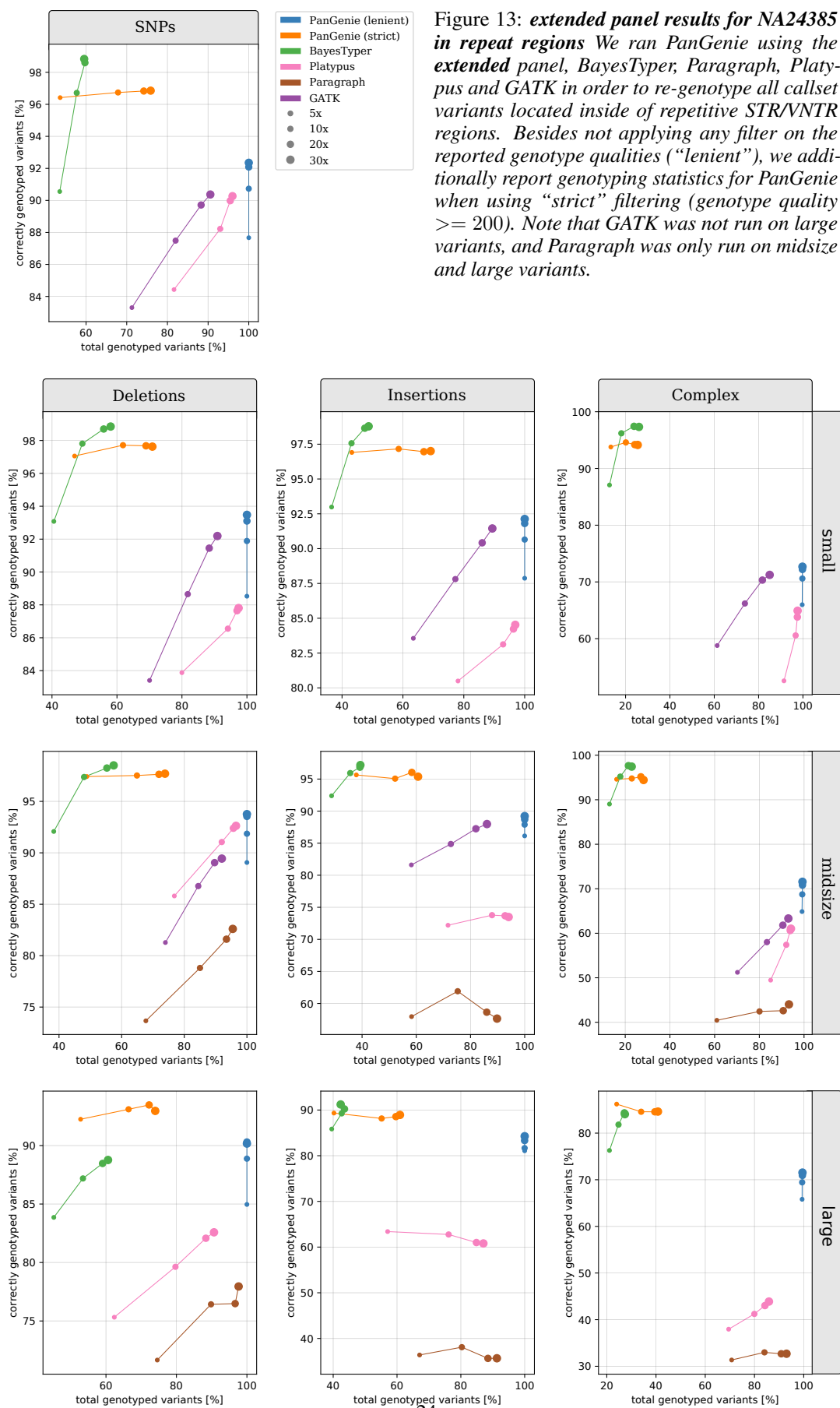


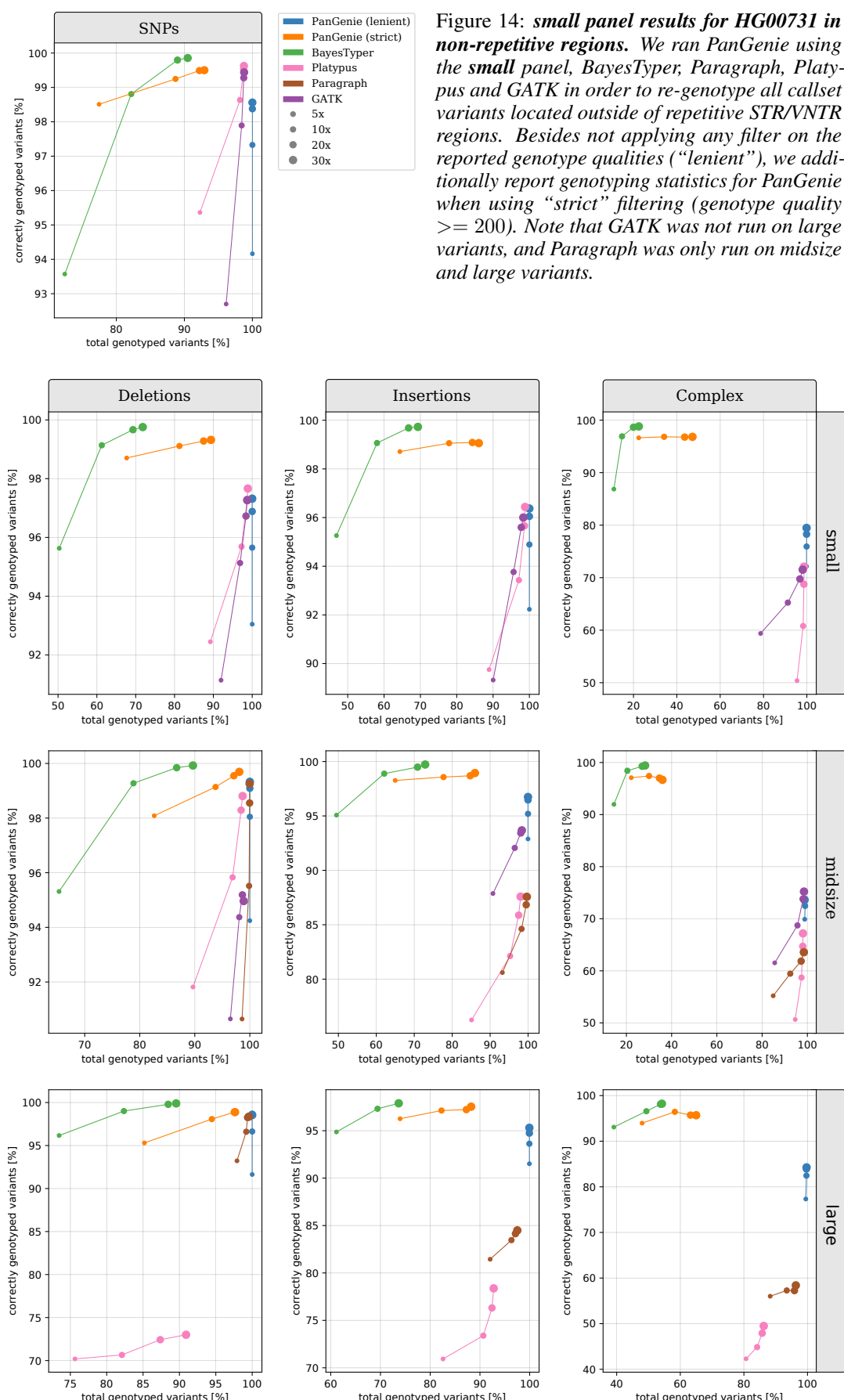


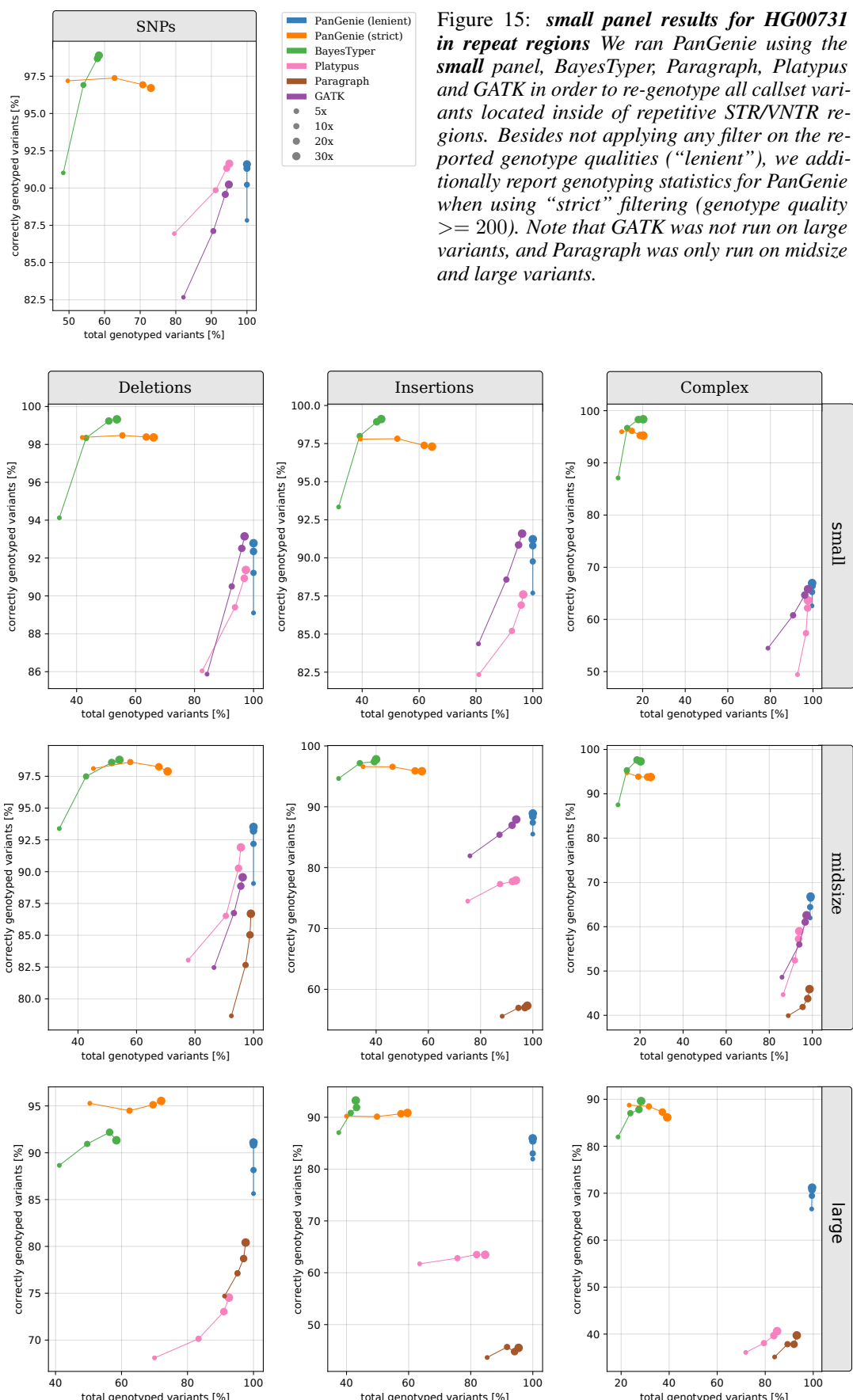


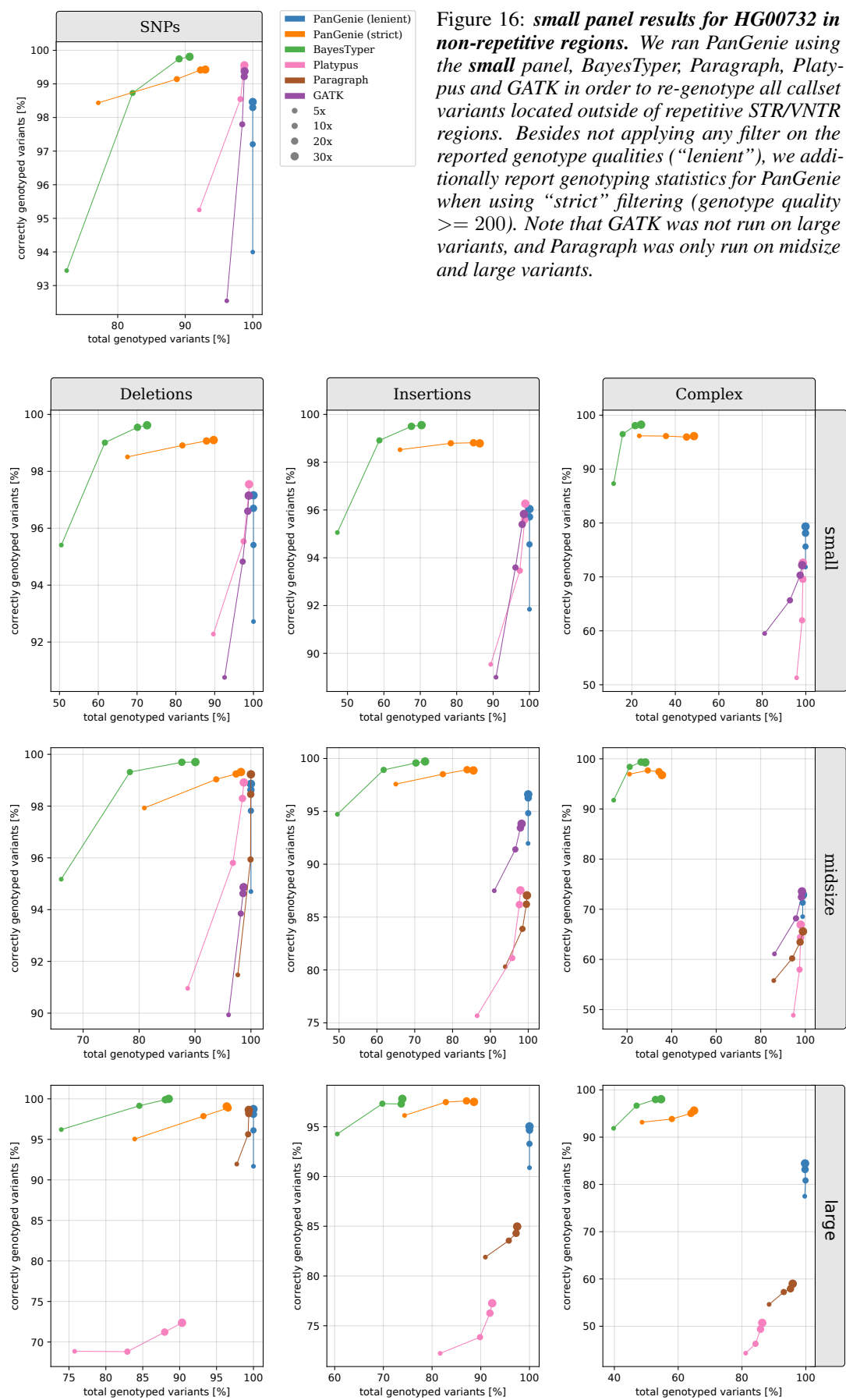


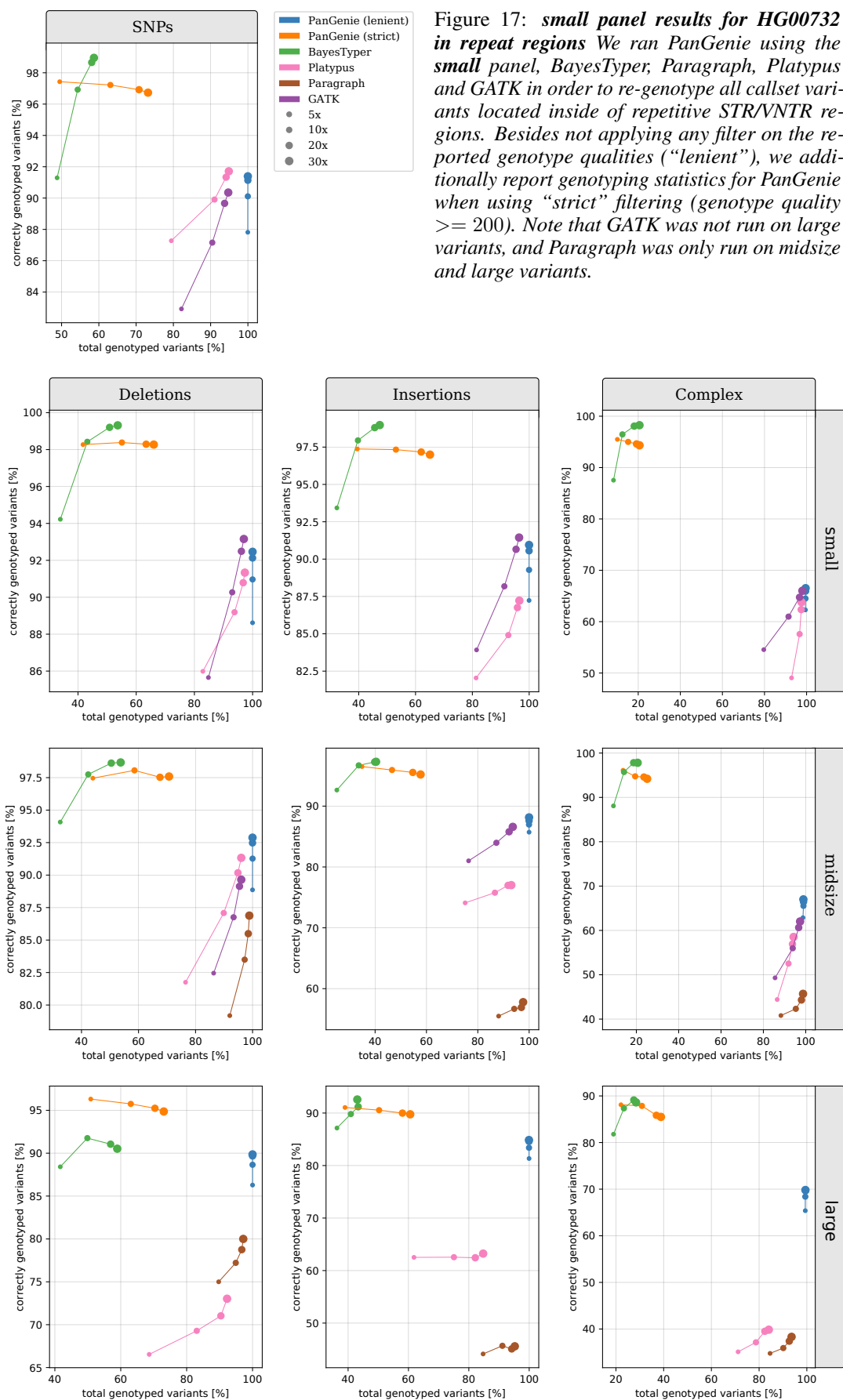


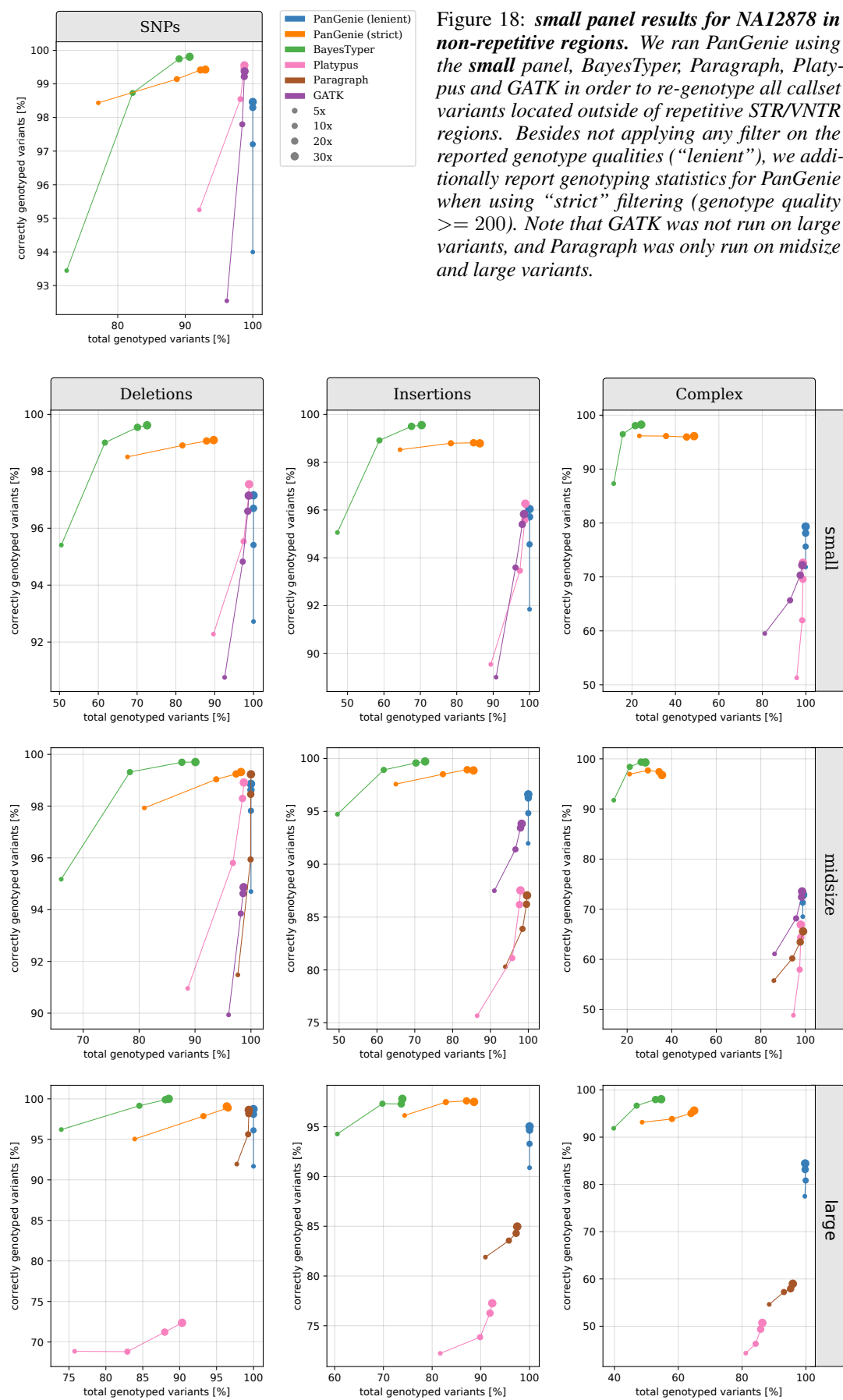


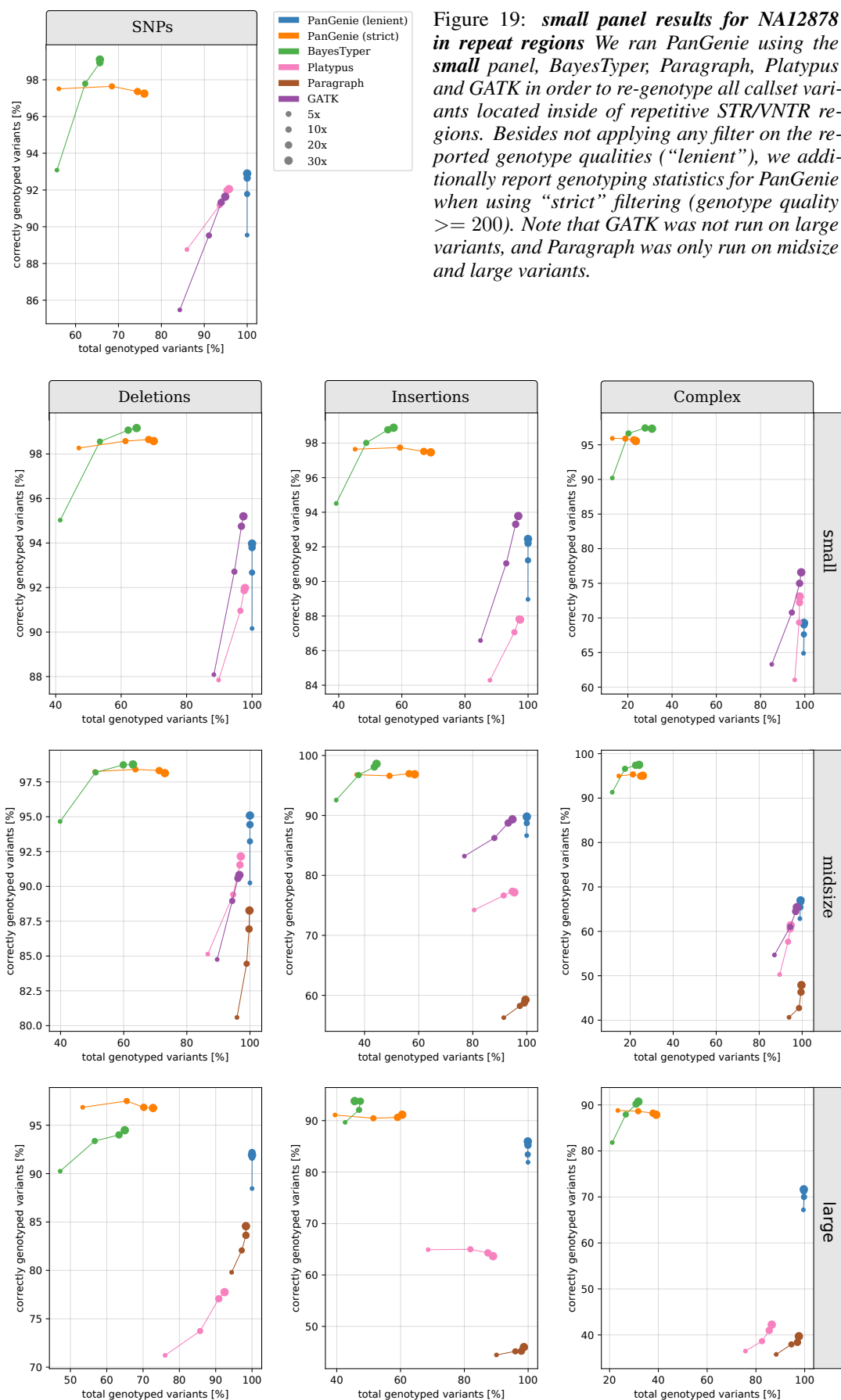


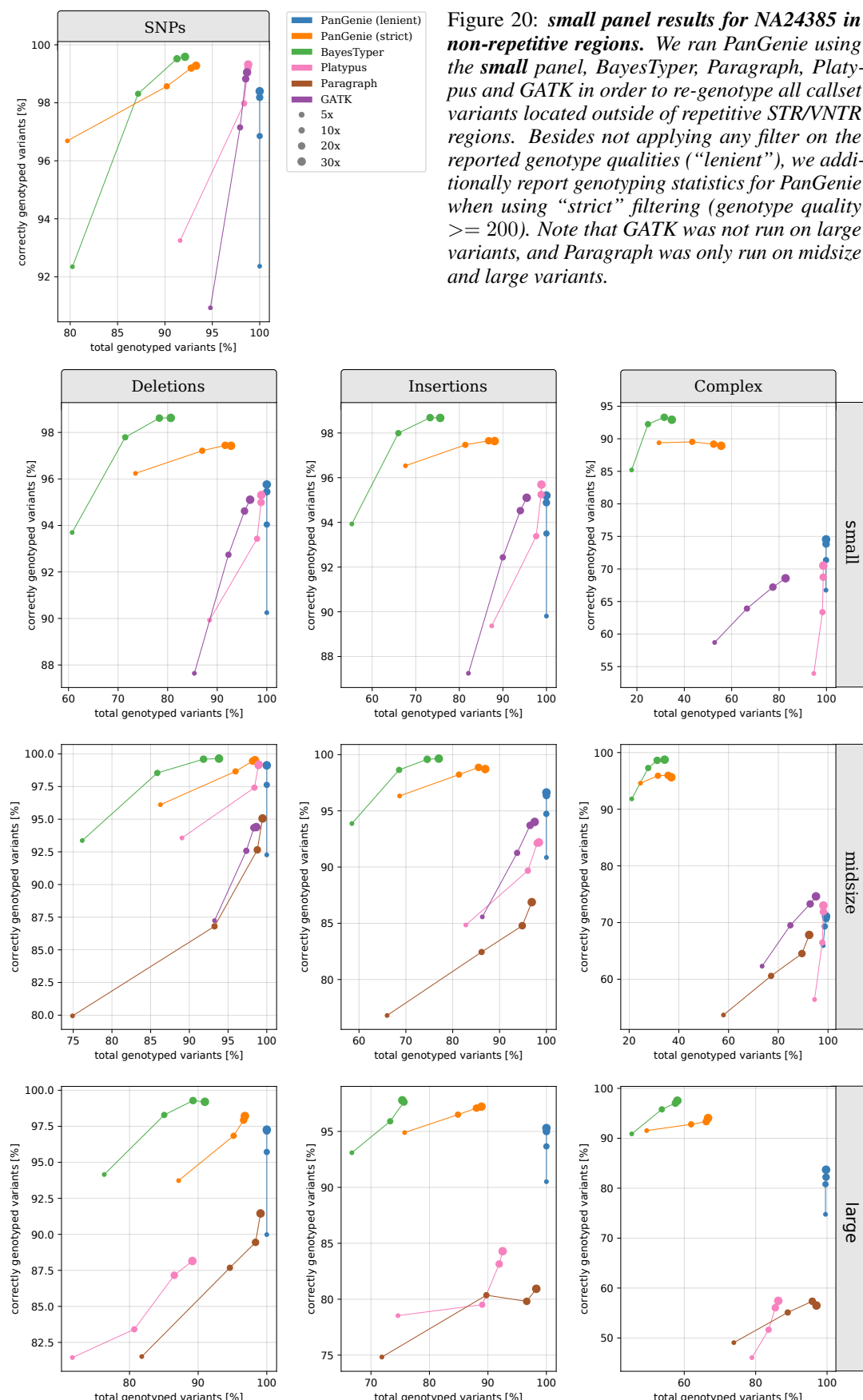


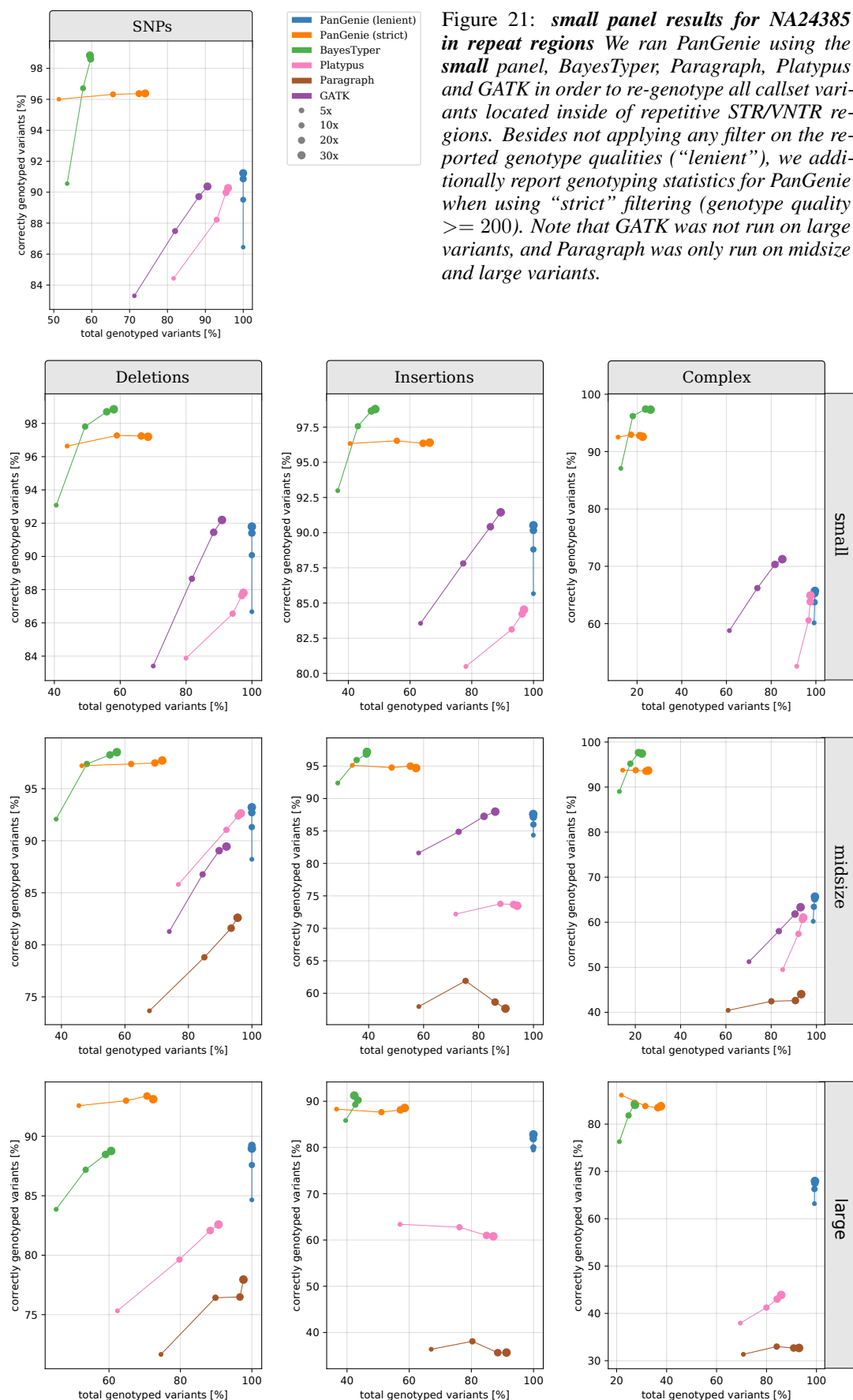












502 **Runtimes** We measured the runtimes of all genotypers for the experiments described in Section 2.3 and show them
 503 in the table below. For all methods we measured the time needed to produce genotypes given the raw, unaligned
 504 sequencing reads. Therefore, runtimes for the mapping based approaches (Platypus, GATK, Paragraph) include the
 505 time that was needed to align the reads to the reference genome.

coverage	method	runtime (CPU sec)			
		HG00731	HG00732	NA12878	NA24385
5	PanGenie-4	5:43:14	5:47:27	5:24:09	5:50:16
	PanGenie-10	16:30:46	16:09:53	16:33:56	16:39:10
	BayesTyper	19:15:14	19:01:26	19:15:50	19:18:32
	bwa + Platypus	20:24:03	20:17:03	17:49:02	20:23:04
	bwa + GATK ¹	47:24:18	46:41:48	43:53:18	46:28:50
	bwa + Paragraph ²	21:49:04	21:42:20	19:42:04	21:58:48
10	PanGenie-4	7:13:16	7:21:35	6:53:07	7:28:14
	PanGenie-10	18:38:24	18:32:37	17:58:22	18:39:40
	BayesTyper	21:06:09	20:48:47	20:44:49	21:32:58
	bwa + Platypus	39:20:30	39:00:07	33:41:37	39:29:54
	bwa + GATK ¹	74:16:30	73:38:42	67:07:30	73:17:21
	bwa + Paragraph ²	42:42:03	42:20:31	38:30:50	43:26:37
20	PanGenie-4	10:34:05	10:17:36	9:03:41	10:16:48
	PanGenie-10	21:58:38	21:12:08	19:39:27	21:24:34
	BayesTyper	23:30:17	23:14:27	22:28:14	24:27:43
	bwa + Platypus	76:55:22	76:40:07	65:51:00	77:35:07
	bwa + GATK ¹	125:25:19	124:35:58	113:03:27	124:42:22
	bwa + Paragraph ²	84:28:32	84:03:30	77:15:57	86:23:53
30	PanGenie-4	14:41:47	17:34:07	12:59:47	14:07:18
	PanGenie-10	26:59:57	26:38:29	23:42:00	23:49:38
	BayesTyper	27:47:37	27:27:24	25:18:09	30:04:13
	bwa + Platypus	115:32:52	114:32:36	95:31:42	115:59:24
	bwa + GATK ¹	177:37:56	175:12:35	152:07:04	175:26:41
	bwa + Paragraph ²	127:27:47	126:00:29	115:11:40	129:51:49

¹ GATK was run on SNPs, small and midsize variants only.

² Paragraph was run on midsize and large variants only.

Table 4: **Runtimes** (in CPU hh:mm:ss) of the different genotyping methods at different coverages.

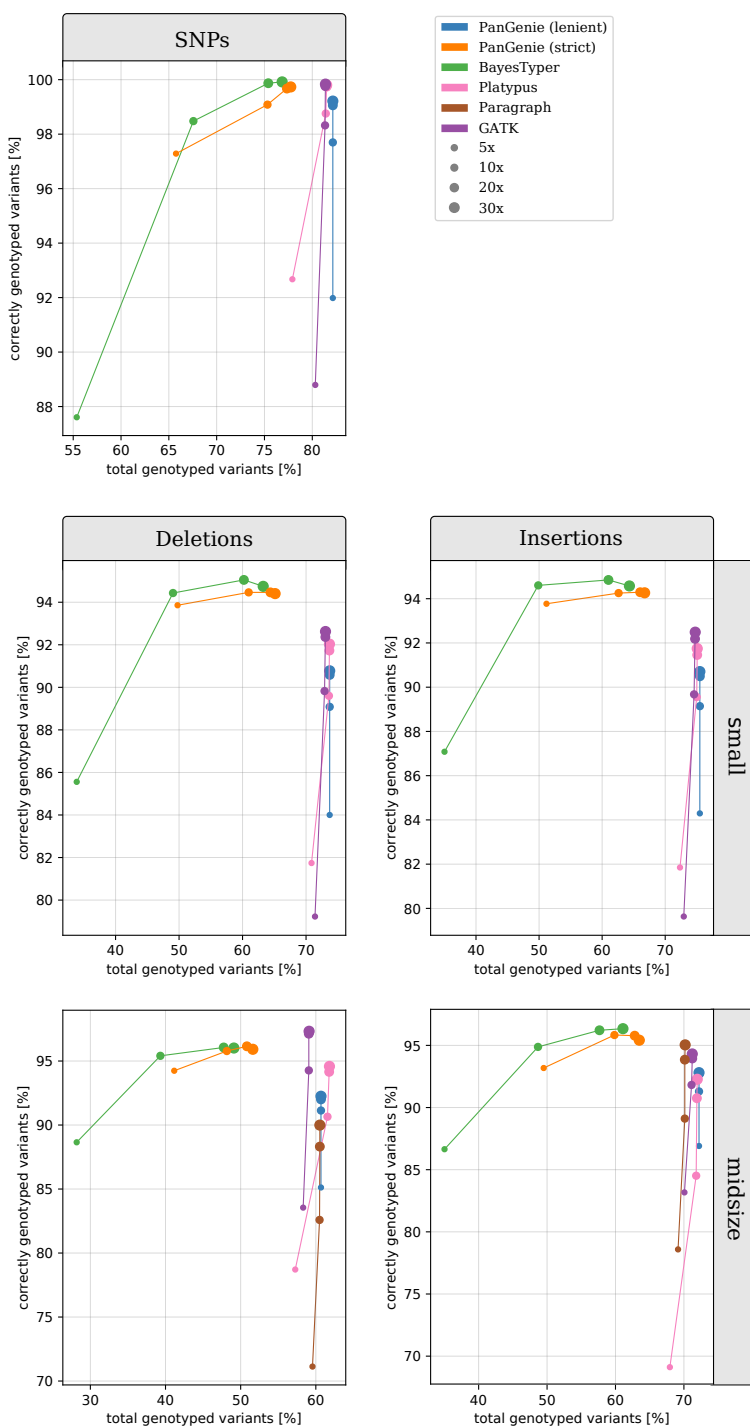


Figure 22: **Genotyping Performance** for sample NA12878 on GIAB variants at different coverages. Evaluation of the genotypes produced by PanGenie, BayesTyper, Paragraph, Platypus and GATK for the variants overlapping with the Genome in a Bottle ground truth.

506 Comparison to GIAB variants

507 We also evaluated our genotyping results for individual NA12878 taking the Genome in a Bottle (GIAB) small variant
 508 calls [43] as a ground truth. We determined all variants that the GIAB callset and our assembly-based VCF had in
 509 common and compared the genotype predictions made by the genotypers to the true genotypes. We only considered
 510 exact matches, that is, a variant was considered an overlap, if the positions and genotype alleles between both callsets
 511 were exactly identical. Figure 22 shows the results. Variants that were present in the GIAB callset but not our assembly
 512 calls, were treated as “untyped” when creating the plots.

	SNPs	small deletions	small insertions	midsize deletions	midsize insertions
GIAB callset	3085616	247499	242711	2658	1925
variants in overlap	2534770	182493	183257	1613	1390
overlap [%]	82,15%	73,73%	75,50%	60,68%	72,21%

Table 5: **GIAB overlap.** Number of variants that overlap with the Genome in a Bottle small variant calls.

variant type	total	no sign. deviation from HWE	
SNPs	5232099	5018638	(95.9%)
small insertions	312904	298518	(95.4%)
small deletions	347425	333018	(95.9%)
midsize insertions	6362	6063	(95.3%)
midsize deletions	6122	5866	(95.8%)
large insertions	4194	3992	(95.2%)
large deletions	2433	2311	(95.0%)
all	5911539	5668406	(95.9%)

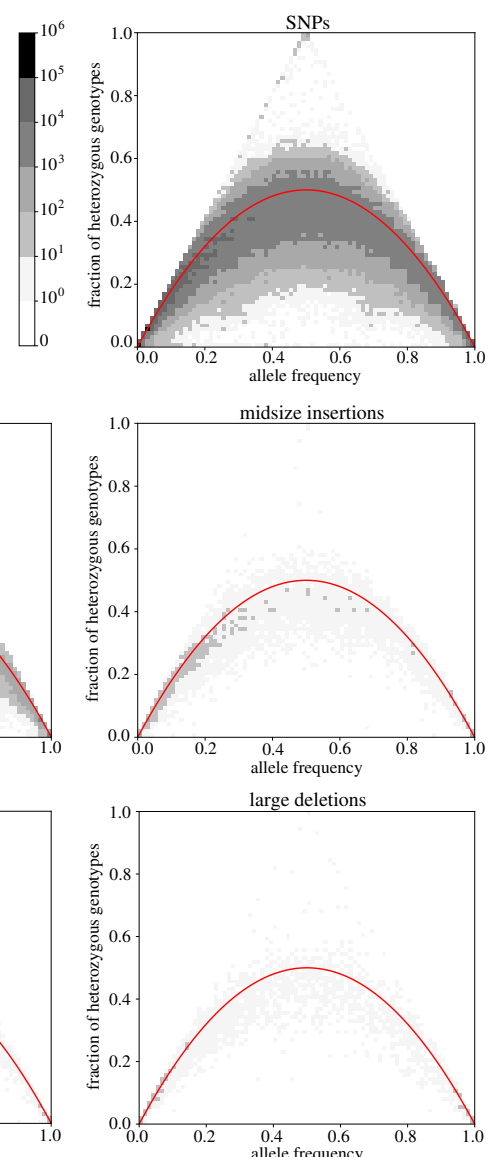


Figure 23: **Genotyping larger cohorts (strict filtering).** The table provides the amount of variants for which no significant deviation from Hardy-Weinberg Equilibrium was observed. Each plot shows the fraction of heterozygous genotypes at a variant position as a function of the allele frequency. The red curve shows what is expected according to Hardy-Weinberg equilibrium. Only genotypes with a quality of at least 200 were considered and positions with more than 10 low quality genotypes were skipped.

513 Genotyping Larger Cohorts

514 Here we additionally show the results for the experiment described in Section 2.4 that we get when using strict filtering
 515 on the reported genotypes. At each biallelic variant position, only genotypes with a quality ≥ 200 were considered.
 516 Additionally, we skip if a genotype quality below that threshold was reported for more than ten samples. Results are
 517 shown in Figure 23.

518 Command lines used for genotyping

519 We used a VCF-file containing the variants detected from the haplotype-resolved assemblies as input variants for all
 520 genotyping tools and genotyped them based on short Illumina reads as described in Section 2.3.

521 We ran BayesTyper (version v1.5) and PanGenie with default parameters using the raw, unaligned Illumina
522 reads (FASTQ format) as input. For BayesTyper, we used the Snakemake pipeline provided in their repository
523 (<https://github.com/bioinformatics-centre/BayesTyper>). PanGenie (https://bitbucket.org/jana_ebler/pangenie/src/master/, commit: f46a9e5) was run based on the command shown below,

525 PGGTyper -i reads.fq -v variants.vcf -r reference.fa -o pangenie-results -j 22 -t 22 -g
526 where variants.vcf refers to the input VCF file that contains the variants to be genotyped.

527 The remaining tools were provided with the aligned reads in BAM format, produced by mapping them to
528 the reference genome using bwa. Platypus (version 0.8.1) was run in re-typing mode with additional options
529 --source=variants.vcf, --minPosterior=0 and --getVariantsFromBAMs=0.

530 In order to run GATK (version 4.1.3.0), we first marked duplicates in our BAMs and then used HaplotypeCaller in
531 re-typing mode in order to compute genotypes for the input variants using the command below. Note that we did not
532 genotype large variants with GATK, therefore we removed them from the input VCF file prior to genotyping.

533 GATK HaplotypeCaller -reference reference.fa --input reads.bam --output GATK-results
534 --minimum-mapping-quality 20 --genotyping-mode GENOTYPE_GIVEN_ALLELES --alleles
535 variants_no_large.vcf

536 In order to run Paragraph, we first computed the depth of the input BAM file using the command

537 /bin/idxdepth -b reads.bam -r reference.fasta -o depth.json

538 and prepared the Manifest file required for genotyping. In the next step, we used the command bin/multigrmpy.py
539 with default parameters in order to genotype the input variants. Note that we removed all variants shorter than 20 bp
540 from the input VCF before running Paragraph in order to only type midsize and large variants.

541 The complete pipeline used to run the evaluation including the commands used to run all tools can be found in this
542 repository: https://bitbucket.org/jana_ebler/genotyping-experiments/src/master/